nature structural & molecular biology

Intrinsic tethering activity of endosomal Rab proteins

Sheng-Ying Lo[1,2], Christopher L Brett[1,5], Rachael L Plemel[1], Marissa Vignali[3], Stanley Fields[3,4], Tamir Gonen[1,4,5] & Alexey J Merz[1]

Rab small G proteins control membrane trafficking events required for many processes including secretion, lipid metabolism, antigen presentation and growth factor signaling. Rabs recruit effectors that mediate diverse functions including vesicle tethering and fusion. However, many mechanistic questions about Rab-regulated vesicle tethering are unresolved. Using chemically defined reaction systems, we discovered that Vps21, a *Saccharomyces cerevisiae* ortholog of mammalian endosomal Rab5, functions in *trans* with itself and with at least two other endosomal Rabs to directly mediate GTP-dependent tethering. Vps21-mediated tethering was stringently and reversibly regulated by an upstream activator, Vps9, and an inhibitor, Gyp1, which were sufficient to drive dynamic cycles of tethering and detethering. These experiments reveal a previously undescribed mode of tethering by endocytic Rabs. In our working model, the intrinsic tethering capacity Vps21 operates in concert with conventional effectors and SNAREs to drive efficient docking and fusion.

Vesicle and organelle tethering are reversible recognition events that precede docking and bilayer fusion. Tethering also mediates transient contacts that allow materials such as lipids to be passed between organelles[1]. The most broadly deployed regulators of tethering are small G proteins of the Rab and Arf families[2,3]. These molecular switches, inactive when GDP bound, become activated upon GTP binding. Rabs are activated by guanosine nucleotide exchange factors (GEFs) that catalyze GDP expulsion to allow GTP binding, and they are inactivated by GTPase accelerating proteins (GAPs) that trigger the hydrolysis of GTP to GDP. Active GTP-bound Rabs recruit effector proteins that execute diverse functions including cytoskeletal transport, activation of lipid kinases, vesicle tethering and SNARE-mediated fusion.

Many Rabs and Rab effectors promote membrane tethering. However, tethering activity has generally been inferred from *in vivo* experiments or from assays using cell extracts or organelles. In these complex reaction systems, hundreds or thousands of molecular species are present; some directly mediate tethering whereas others act as upstream regulators that promote tethering but do not directly mediate it. For example, mammalian Rab5 regulates homotypic tethering and fusion of endosomes[4–9]. Rab5 promotes phosphatidylinositol-3-kinase activity that in turn generates binding sites for other molecules that mediate tethering, including the Rab5 effector EEA1 (refs. 10–12). EEA1 binding to 3-phosphoinositides is essential for its tethering activity *in vivo*. However, mutations in EEA1 that abrogate its high-affinity interactions with Rab5 do not interfere with EEA1 membrane association or endosome tethering. Instead, these mutations act downstream of tethering to block homotypic fusion[13]. Thus, although both Rab5 and EEA1 are unambiguously involved in endosome tethering, it remains uncertain whether Rab5 promotes tethering mainly by serving as a mechanical anchor for EEA1 (that is, Rab5 is part of the core tethering machinery), or whether the major role of Rab5 is to send instructive signals to other core tethering factors. There are similar uncertainties for the yeast Rab5 ortholog Vps21 and its effectors, and for the vast majority of other Rab-effector systems.

A central challenge in biochemistry is to reconstitute key biological processes using purified components, so as to define minimal reaction systems and explore their modes of action (for example, refs. 14–17). So far, only a handful of proteins have mediated tethering in chemically defined systems. These include GMAP-210, an effector of Arf1 at the Golgi[18], and HOPS, an effector of Ypt7 at the yeast vacuole[19–21]. For the vast majority of effectors currently known to promote tethering, it is uncertain whether their modes of action are mechanical or regulatory. Thus, the development of quantitative approaches to analyze the activities of putative tethering factors, especially factors that interact with Rabs, is a major goal in the field. While developing a general set of methods for this purpose, we discovered that Vps21 and other endosomal Rab proteins in *S. cerevisiae* not only bind classical effectors[22–27] but also undergo GTP-regulated Rab-Rab interactions that directly drive tethering *in vitro*, completely without effectors. These findings reveal a previously unknown intrinsic activity of endosomal Rabs in *S. cerevisiae*, and they suggest the presence of an additional layer of membrane-membrane recognition events in endosomal membrane traffic.

[1]Department of Biochemistry, University of Washington School of Medicine, Seattle, Washington, USA. [2]Department of Chemistry, University of Washington, Seattle, Washington, USA. [3]Department of Genome Sciences, University of Washington School of Medicine, Seattle, Washington, USA. [4]Howard Hughes Medical Institute, University of Washington School of Medicine, Seattle, Washington, USA. [5]Present addresses: Department of Biology, Concordia University, Montreal, Quebec, Canada (C.L.B.); and Janelia Farm Research Campus, Howard Hughes Medical Institute, Ashburn, Virginia, USA (T.G.). Correspondence should be addressed to A.J.M. (merza@uw.edu).

Received 30 May 2010; accepted 22 September 2011; published online 11 December 2011; doi:10.1038/nsmb.2162

RESULTS

Vps21-GTP tethers without Rab effectors

To directly and quantitatively evaluate the tethering capabilities and mechanisms of Rabs and effectors, we developed liposome-based *in vitro* systems. Native Rab proteins generally comprise a compact globular N-terminal GTP-binding domain and a C-terminal intrinsically disordered hypervariable domain of ~30 residues. Rabs associate with membranes through two geranylgeranyl lipids that are covalently attached to the extreme C terminus of the hypervariable domain. In our experiments, this lipid anchor was replaced by a C-terminal polyhistidine tag, which binds avidly to a synthetic lipid, Ni^{2+}-1,2-dioleoyl-*sn*-glycero-3-[*N*(5-amino-1-carboxypentyl)iminodiacetic acid)succinyl] (Ni^{2+}-NTA-DOGS). We prepared liposomes (~100-nm diameter) doped with Ni^{2+}-NTA-DOGS by extrusion, and then we decorated the liposomes with C-terminally His_{10}-tagged Rabs (**Fig. 1a**; see also ref. 28). We measured liposome tethering by quasielastic light scattering (QLS), which reports tethering in real time as an increase in effective particle diameter. The response of the QLS system was validated using mixtures of extruded liposomes of different diameters (see **Supplementary Methods**).

Unexpectedly, we observed robust GTP-dependent increases in effective particle diameter when liposomes were decorated with the *S. cerevisiae* endosomal Rab Vps21, without additional effector proteins (**Fig. 1b**). This particle size increase was nearly eliminated when Vps21 was preloaded with GDP rather than GTP, or when liposomes were decorated with the vacuolar-lysosomal Rab Ypt7. Because the particle size increases reported by QLS might have been due to either liposome tethering or membrane fusion, we examined aliquots from the liposome preparations by negative-stain transmission EM (TEM; **Fig. 1c**). TEM showed massive clusters of Vps21-GTP–decorated liposomes, but there was no evident size increase of individual liposomes within the clusters. Similarly, light microscopic observations of suspensions of fluorescently labeled liposomes in aqueous buffer (**Fig. 1d**) showed thousands of visible clusters in the presence of Vps21-GTP. After 40 min of incubation, the diffuse fluorescent background of individual, fast-diffusing Vps21-GTP liposomes was markedly depleted, indicating that most of the liposomes in the starting population were tethered within large clusters. These observations indicate that the Vps21-GTP liposome clusters seen by TEM formed in aqueous suspension, prior to deposition on the grid and negative staining. In sharp contrast to the tethering seen with Vps21-GTP, liposomes decorated with Vps21-GDP or liposomes decorated with Ypt7 bound to either GDP or GTP (**Fig. 1c**,**d**) did not form large clusters when examined by light microscopy or EM. Thus, three independent lines of evidence (QLS, TEM and fluorescence microscopy) indicate that Vps21-GTP drives efficient Rab-selective and GTP-dependent liposome tethering *in vitro*.

Tethering occurs at physiological Rab surface densities

To further characterize Vps21-mediated tethering, we titrated Rabs and lipids (**Fig. 2a**,**b** and **Supplementary Fig. 1**). The Ni^{2+} chelator lipid NTA-DOGS is anionic. The nitrilotriacetic acid (NTA) moiety has a net charge of –3, and it binds Ni^{2+} with 1:1 stoichiometry[29]. Ni^{2+}-NTA-DOGS-doped liposomes, like endocytic organelles, therefore have a net negative charge. Over a range of Ni^{2+}-NTA-DOGS concentrations, we observed strong tethering signals at Vps21-His_{10} surface densities of 1,500–7,000 μm^{-2}. In a comparable *in vitro* reconstitution of liposome tethering by another small G protein, Arf1, and its effector GMAP, tethering has been observed at Arf1 densities of 8,000–14,000 μm^{-2} and GMAP densities of 700–7,000 μm^{-2} (ref. 18). Notably, we found that tethering was highly responsive to the Vps21-GTP surface density (**Supplementary Fig. 1a**; Hill coefficient

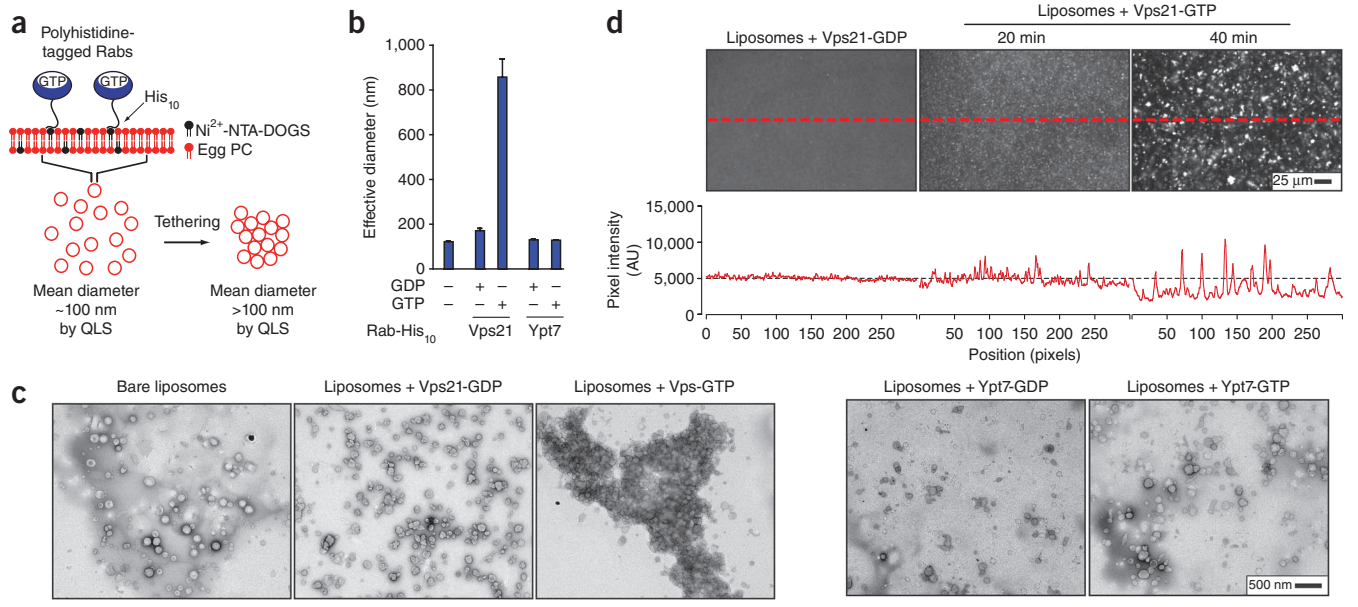

Figure 1 GTP-bound Vps21 tethers liposomes. (**a**) Experimental configuration. Full details are in Online Methods and **Supplementary Methods**. (**b**) Liposome particle size distributions were measured by QLS after 60-min incubation in the presence of the indicated Rab-His_{10} proteins, preloaded with GDP or GTP. Error bars indicate mean and s.e.m. for three independent experiments. (**c**) TEM images of negatively stained samples taken from experiment in **b**. (**d**) Liposomes were prepared as in **a**–**c**, except that fluorescent lipid was incorporated. Liposomes were incubated for 20 or 40 min, then a drop of the suspension was imaged by epifluorescence microscopy (200 ms exposure). Brightness and contrast adjustments are identical for the panels shown. Traces below the images show pixel intensities along the indicated dashed lines (AU, arbitrary units). Untethered liposomes are small and move rapidly and appear as diffuse fluorescence. As tethering proceeds, clusters grow in size and the fluorescent background markedly decreases indicating that most individual liposomes in the population have tethered. Liposomes with GDP- His_{10}-Vps21 are shown at 20 min incubation and were indistinguishable from those at 40 min incubation.

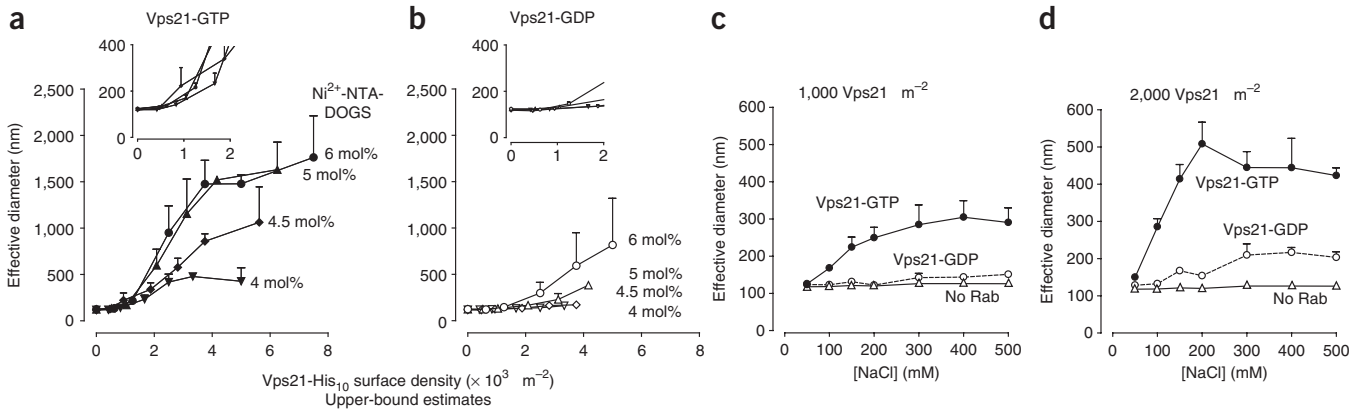

Figure 2 Vps21 surface density and tethering activity. (**a**,**b**) Liposome tethering, measured by QLS, was examined as a function of Vps21 membrane surface density. Vps21 was loaded with GTP (**a**) or GDP (**b**). Insets, onset of tethering at low Vps21 surface densities. Additional surface density data for Vps21 and Ypt7 are in **Supplementary Figure 1**. (**c**,**d**) To test effect of ionic strength, liposomes were decorated with Vps21-GDP or Vps21-GTP at two different surface densities, and tethering was monitored by QLS in buffers containing indicated salt concentrations. As in **a**,**b**, indicated Vps21 surface densities are upper-bound estimates. Data are mean and s.e.m. from three independent experiments.

≥3.5, 95% confidence limit). A simple interpretation of this dosage hypersensitivity is that tethering occurs through a cooperative mechanism that entails the concerted action of several Vps21-GTP complexes. Tethering was markedly lower when liposomes were decorated with inactive Vps21-GDP (**Fig. 2a**,**b** and **Supplementary Fig. 1b**). At very high ratios of Vps21-His_{10} to Ni^{2+}-NTA-DOGS, tethering was inhibited, probably through competitive inhibition by unbound Vps21-His_{10} (**Supplementary Fig. 1b**). With the vacuolar Rab Ypt7 (**Supplementary Fig. 1c**), we did not observe tethering at any concentration of Ni^{2+}-NTA-DOGS or Ypt7. This result is consistent with the demonstrated requirement for the HOPS effector complex in Ypt7-mediated tethering[19–21] and underscores the selectivity of Vps21-mediated tethering.

We next sought to determine whether Vps21-mediated tethering occurs within a physiologically relevant span of surface densities. To provide a criterion for the onset of tethering, we defined the critical surface density for tethering as the density of surface-bound Rab at which the effective particle diameter, measured by QLS, increases to twice the effective diameter of bare, untethered control liposomes. Nominally, at the critical surface density each liposome is on average tethered to one other liposome. The critical surface density for tethering by Vps21-GTP was ≤1,300 μm^{-2} (**Fig. 2a**,**b**, insets). This density corresponds to ~40 Vps21 molecules on the surface of an endosome of 100 nm diameter, or ~10 molecules on a 50-nm endosome. These are upper-bound estimates that assume that every Vps21 molecule in the assay system is both active and bound to a liposome. Although the Vps21 surface density on endosomes *in vivo* is unknown, estimates are available for the surface densities of two other Rabs. The density of Ypt7 on the *S. cerevisiae* vacuole is ~500 μm^{-2}, and the density of Rab3a on mammalian synaptic vesicles is ~1,950 μm^{-2} (**Supplementary Methods**; refs. 30–32). GTP-regulated tethering by Vps21 therefore occurs within the physiologically relevant range of Rab surface densities. Below this range detectable tethering does not occur, whereas above this range regulation by GTP binding is attenuated and tethering occurs constitutively.

To further characterize the interactions that drive Vps21-mediated tethering, we carried out QLS-based tethering assays across a range of salt concentrations (**Fig. 2c**,**d**). At subphysiological ionic strengths, tethering was potently inhibited. As the buffer ionic strength increased, the efficiency of tethering increased and then leveled off. Under all ionic conditions tested, we observed GTP selectivity, but the highest selectivity was at physiological ionic strength (150–200 mM NaCl). Inefficient tethering at low ionic strength could result from low shielding of the electrostatic repulsion between the negatively charged liposomes, or from decreased hydrophobic forces at protein interaction surfaces .

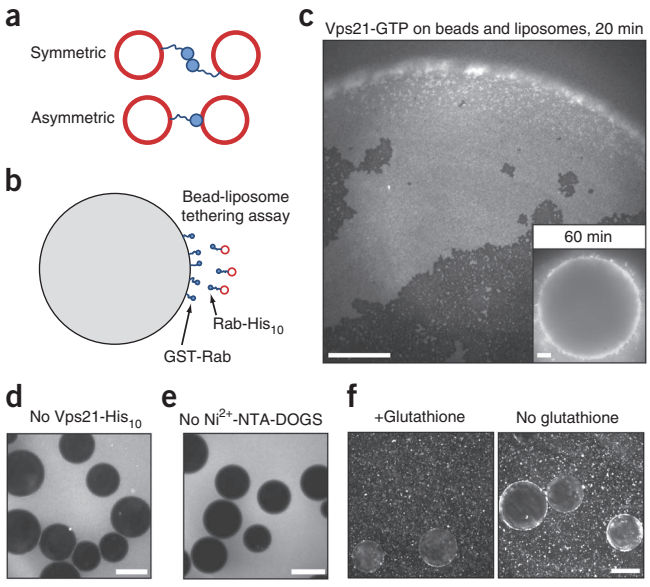

Figure 3 Vps21 interactions in *trans* are required for efficient tethering. (**a**) Schematic of two possible mechanisms of Rab-mediated tethering. (**b**) Schematic of bead-liposome tethering assay. (**c**) GTP-loaded GST–Vps21 beads were photographed after incubation for 20 or 60 min in presence of fluorescent liposomes containing 6 mol% Ni^{2+}-NTA-DOGS and GTP-loaded Vps21-His_{10}. Images are representative of nine independent experiments. (**d**) As in **c** (inset) but without GTP-loaded Vps21-His_{10}. (**e**) As in **c** (inset), but liposomes were prepared without Ni^{2+}-NTA-DOGS. (**f**) As in **c**, except that after 20 min incubation, 10 mM reduced glutathione was added (left), or buffer without glutathione was added (right). Samples were then incubated for 4 min more, then photographed. Scale bars, 15 μm (**c**) and 75 μm (**d**–**f**).

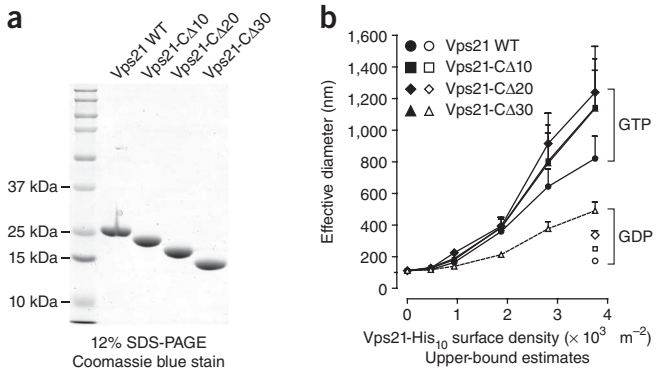

Figure 4 The Vps21 C-terminal linker is not required for tethering. (**a**) Vps21-His_{10} fusion proteins lacking last 10, 20 or 30 residues of the Vps21 C-terminal linker were prepared. Purified proteins (5 μg) were analyzed by SDS-PAGE. (**b**) Liposomes bearing these proteins were assayed by QLS for the ability to drive tethering over indicated range of surface densities. Each construct was loaded with either GTP (filled symbols) or GDP (open symbols). Liposomes contained 4.5 mol% Ni^{2+}-NTA-DOGS. Error bars indicate mean and s.e.m. from four independent experiments.

Rab-Rab interactions in *trans* drive efficient tethering

In principle, Vps21-mediated tethering might occur through either a symmetric or an asymmetric mechanism (**Fig. 3a**). In the symmetric mechanism, Vps21 anchored to opposite membranes would dimerize or oligomerize in *trans* to drive tethering. This mechanism depends on protein-protein contacts. In the asymmetric mechanism, a single Vps21 molecule anchored to one vesicle would undergo GTP-triggered direct binding to the lipids of the opposite vesicle. It is also possible that both classes of mechanisms could contribute to Vps21-mediated tethering.

To assess these hypotheses, we used a bead-liposome assay that allows the components on two tethering surfaces to be varied independently (**Fig. 3b**). A similar system has been used to probe the binding of nucleoporin proteins to phospholipid bilayers[33]. Large (~100 μm) glutathione-agarose beads were decorated with glutathione-*S*-transferase (GST)-Rab fusion proteins. The beads were mixed with a suspension of small (~100 nm) fluorescent liposomes with Rab-His_{10} proteins. Tethering of the liposomes to the beads was evident by epifluorescence microscopy as a fluorescent halo at the beads' surfaces (**Fig. 3c**). Using this assay, we found that efficient tethering requires GTP-bound Vps21 anchored to both partner surfaces. Tethering did not occur without Vps21-His_{10} (**Fig. 3d**) or when Vps21-His_{10} attachment to liposomes was prevented by omission of Ni^{2+}-NTA-DOGS (**Fig. 3e**). Similarly, tethered liposomes fell off of the beads when GST-Vps21 was dissociated from the beads by soluble glutathione (**Fig. 3f**). Tethering was also abrogated when Ypt7 replaced Vps21 on either the beads or the liposomes (**Supplementary Fig. 2a**). The inability of bead-bound GST-Vps21 to tether either bare liposomes or liposomes bearing Ypt7 is evidence against asymmetric tethering mechanisms in which GTP binding triggers a Vps21 interaction solely by interacting with the *trans* bilayer. Moreover, substitution of GDP for GTP on GST-Vps21 (beads), on Vps21-His_{10} (liposomes) or on both substantially attenuated tethering (**Supplementary Fig. 2b**). Thus for optimal tethering, Rabs on both partner surfaces must be activated. This result mirrors the symmetrical requirement for activated Rab5-GTP in homotypic docking and fusion of mammalian endosomes[9]. In sum, these results support models in which symmetrical Vps21-Vps21 contacts in *trans* are required for tethering. However, we have so far not detected Vps21 dimerization or oligomerization in solution-based assays (for example, **Supplementary Fig. 3**). Together, these results suggest that restraining Vps21 on a two-dimensional membrane surface may increase avidity to drive tethering. It is also possible, however, that affinity components derived from both protein-membrane and protein-protein interactions are required for efficient tethering (see Discussion).

The Vps21 C-terminal linker is not required for tethering

Native Vps21, like most other Rabs, consists of a compact N-terminal GTP-binding domain that attaches to membranes through a disordered ~30-residue C-terminal linker bearing a doubly geranylgeranylated membrane anchor at its extreme C terminus. To ascertain whether the Vps21 C-terminal linker contributes to tethering, we prepared a set of Vps21-His_{10} mutants with truncated C-terminal linkers (**Fig. 4a**) and evaluated the capacity of these mutants to promote liposome tethering in the QLS assay (**Fig. 4b**). Each of the mutants mediated GTP-dependent tethering with efficiency equivalent to or greater than that of full-length Vps21. Thus, the C-terminal linker domain is not directly involved in the tethering reaction.

Vps21 interacts with other endosomal Rabs to drive tethering

Taken together, our biochemical studies suggest that efficient Vps21-mediated tethering involves a protein-protein interaction, GTP-stimulated Vps21-Vps21 association in *trans*. Unbiased yeast two-hybrid screens provided additional evidence that Vps21 interacts with itself and also with other endosomal Rabs.

In a separate project, we sought to identify new Rab-interacting proteins by carrying out systematic yeast two-hybrid screens. In all our yeast two-hybrid experiments, we used low-copy rather than high-copy vectors, and we carried out the read-out growth assays with 3-aminotriazole, conditions that almost eliminate false positives[34,35]. Using the 11 *S. cerevisiae* Rabs as baits, we interrogated ordered prey arrays containing >5,000 *S. cerevisiae* open reading frames. More than 65,000 crosses yielded ~340 candidate interactions. Among these interactions were many expected Rab interactions with known Rab effectors (ref. 36 and unpublished results), and there were interactions we expected with Rab-specific chaperones, including Rab GDP dissociation inhibitor, Rab escort protein and Yif and Yip proteins (**Supplementary Table 1**). To our surprise, however, the screen repeatedly identified homotypic and heterotypic Rab-Rab interactions among endosomal Rabs. In our initial screens, we detected the Rab5 orthologs Vps21, Ypt52, Ypt53 and Ypt10, the

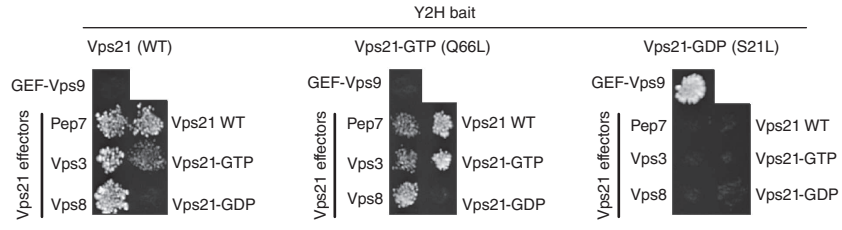

Figure 5 Vps21-GTP interacts with known effectors and with itself in yeast two-hybrid assays. A positive interaction in the yeast two-hybrid assay is indicated by yeast colony growth on medium lacking tryptophan, leucine and histidine, and supplemented with 1.5 mM 3-aminotriazole. The Vps21 effectors Vac1 (also known as Pep7), Vps3 and Vps8 are positive controls for interaction selectivity with Vps21-GTP, whereas Vps9 is a control for interaction selectivity with Vps21-GDP.

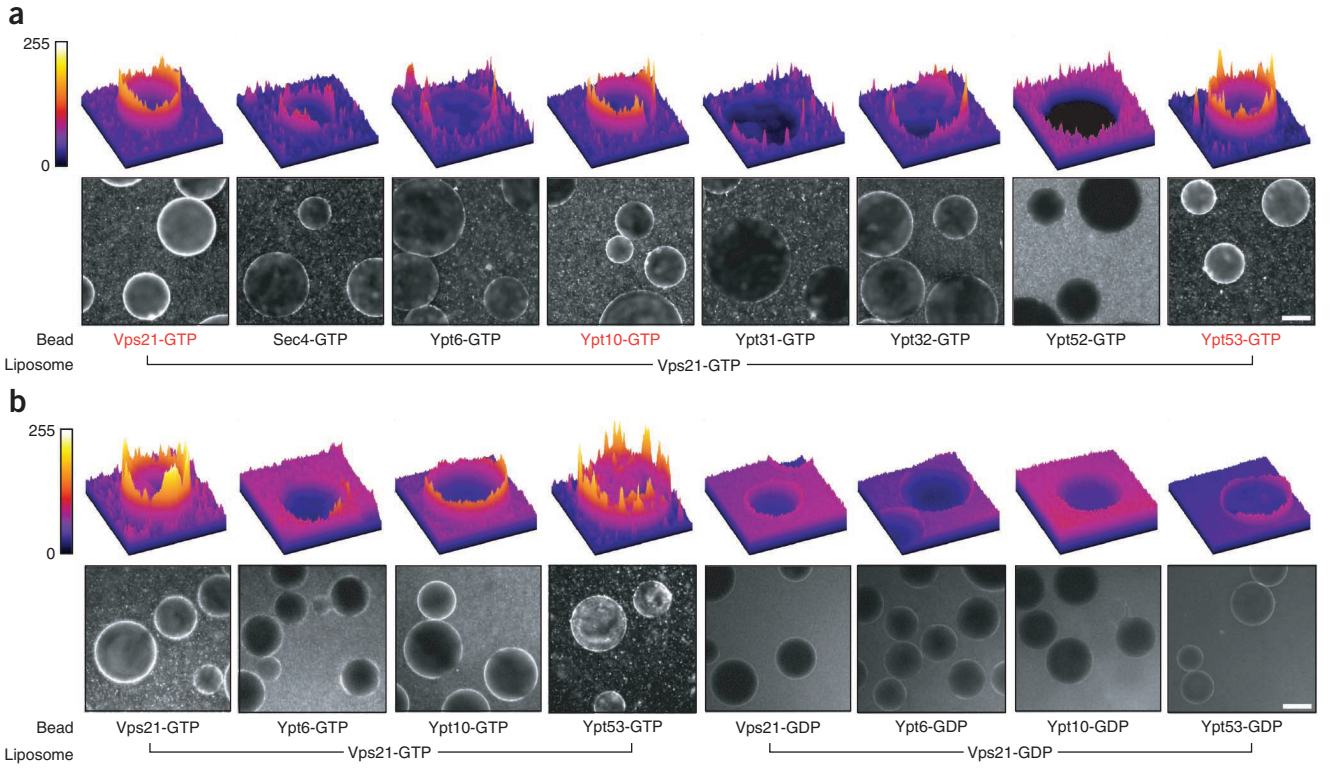

Figure 6 Vps21 interacts with Ypt53 and Ypt10 to drive GTP-dependent heterotypic tethering. (**a**) Heterotypic Rab-Rab tethering was assayed as in **Figure 3** except that beads were decorated with various GTP-loaded GST-Rab fusion proteins, as indicated. Bottom, representative fields of beads under epifluorescence illumination. Top, fluorescence intensity profile plots of representative beads. (**b**) Assays were done as in **a**, except that the Rabs were preloaded with either GTP or GDP. Ypt6, which does not interact with Vps21, was a negative control. Scale bars, 75 μm.

Rab6 ortholog Ypt6 and the Rab 7 ortholog Ypt7 in heterotypic and homotypic Rab-Rab interactions (**Supplementary Table 1**). Moreover, physical interactions among Vps21, Ypt52 and Ypt53 have been independently reported in high-throughput proteomic surveys[37], and mammalian Rab5 isoforms have been reported to undergo GTP-dependent dimerization[38].

In focused yeast two-hybrid assays using independently constructed prey vectors, most of the interactions detected in the high-throughput screens were reproduced and extended (**Supplementary Table 2**), with the Vps21 self-interaction yielding a robust signal (**Fig. 5** and **Supplementary Tables 2** and **3**). Notably, Vps21 interactions with itself and with other Rabs were restricted to wild-type Vps21 and the dominant-active mutant Vps21 Q66L. Moreover, these yeast two-hybrid interactions were similar in signal strength and nucleotide selectivity to Vps21 interactions with its three known effectors, Vps3, Vps8 and Vac1 (refs. 22,23,27,39). We did not observe Rab-Rab or Rab-effector interactions when either bait or prey was the GDP-biased mutant Vps21 S21L. As we expected, the Vps21 S21L mutant robustly interacted with the Vps21 nucleotide exchange factor Vps9 (ref. 40) but not with Vps21 effector proteins. These yeast two-hybrid data provide evidence for GTP-dependent interactions among multiple yeast endosomal Rab proteins and buttress our biochemical results showing that Vps21-mediated tethering is driven by homotypic interactions between activated, membrane-anchored Vps21 molecules.

To ascertain whether heterotypic interactions between Vps21 and other Rabs can drive tethering, as suggested by the yeast two-hybrid results, we used the bead-liposome assay (**Fig. 6**). Beads decorated with various GST-Rab fusions were mixed with fluorescent liposomes bearing Vps21-His_{10}. In these assays (**Fig. 6a**), tethering was mediated by Vps21-GTP with Ypt53 or Ypt10, two other Rabs of the endosomal Rab5 group[41]. In each case, substitution of GDP for GTP abrogated tethering (**Fig. 6b**). Several other Rabs including another Rab5 paralog, Ypt52, did not mediate heterotypic tethering with Vps21 (**Fig. 6a**). Because Vps21-GTP liposomes can interact with one another, there may be competition between Vps21 on the liposomes and the Rabs shown on the beads, reducing the apparent heterotypic tethering signal between Vps21 and any Rabs that Vps21 binds with lower affinity than the self-interaction. This type of competition, if it did occur, would make the bead-liposome assay more stringent and could prevent detection of weaker Rab-Rab tethers. Taken together, the yeast two-hybrid experiments and tethering assays reveal a network of GTP-stimulated homotypic and heterotypic interactions among endosomal Rabs. A subset of these pairs can mediate GTP-dependent tethering *in vitro*.

Regulation of tethering by Vps21 GEF and GAP

Regulation and reversibility are hallmarks of Rab-controlled tethering reactions. Upstream regulators of Vps21 include Vps9, a GEF[40], and Gyp1, a GAP[42,43]. We therefore evaluated whether Vps9 and the Gyp1 catalytic core $Gyp1_{TBC}$ can control Vps21-mediated tethering. Using solution-phase assays, we first verified the catalytic activities of our Vps9 and $Gyp1_{TBC}$ preparations (**Supplementary Fig. 4**). We then investigated whether Vps9 could stimulate tethering by promoting nucleotide exchange. Liposomes bearing Vps21-GDP, monitored by QLS, tethered when both GTP and Vps9 were added to the reactions (**Fig. 7a**). Next, we examined the reversibility of tethering. When added to pretethered liposomes bearing Vps21-GTP, the GAP $Gyp1_{TBC}$ efficiently reversed tethering, again with dose-dependent kinetics at concentrations as low as 10 nM (**Fig. 7b**). The catalytically

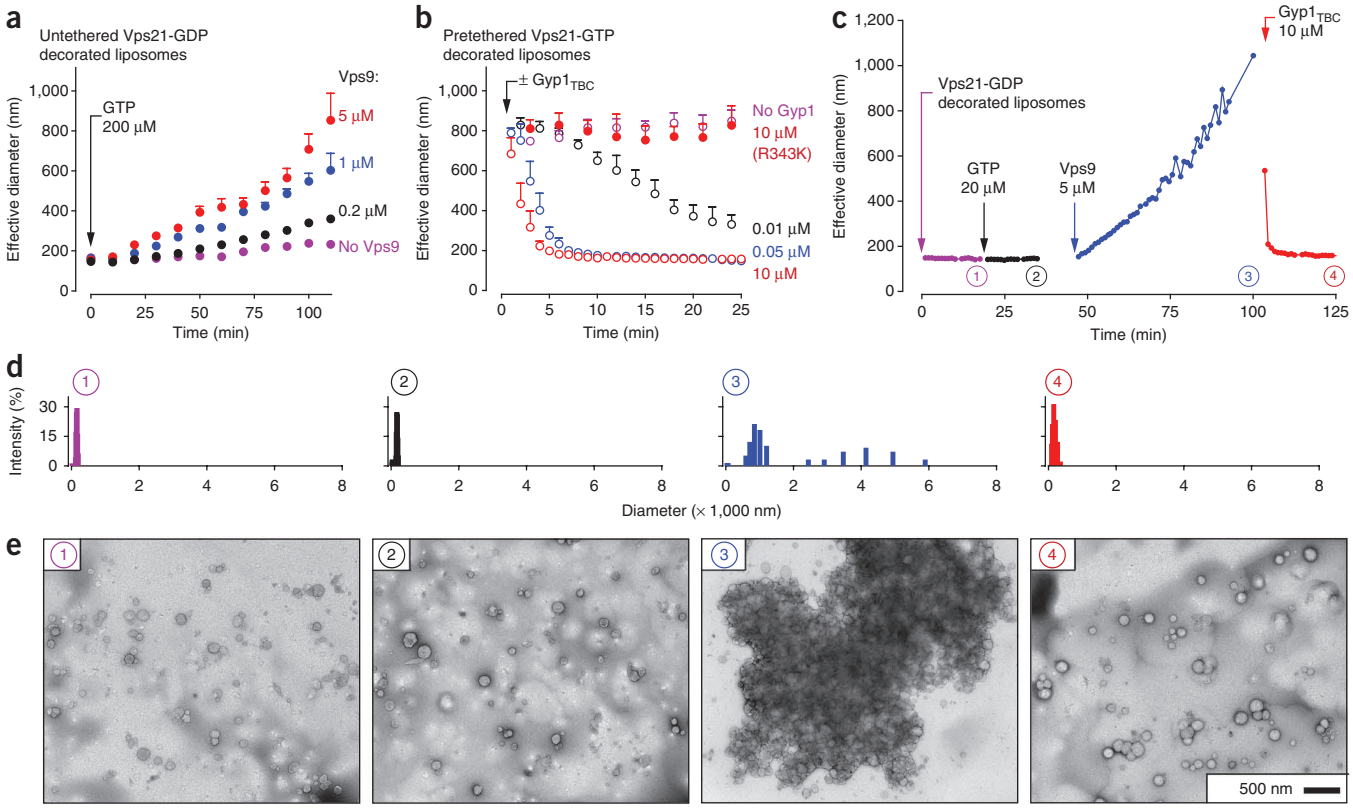

Figure 7 Regulation and reversibility of Vps21-mediated liposome tethering. (**a**) GEF-stimulated tethering. Tethering by GDP-loaded Vps21-decorated liposomes was measured by QLS after addition of 0.2 mM GTP and varying concentrations of Vps9. Data are mean and s.e.m.; data points from three independent experiments were binned into 10-min intervals. (**b**) GAP-mediated reversal of tethering. GTP-loaded Vps21-decorated liposome tethering was measured by QLS after addition of $Gyp1_{TBC}$ or $Gyp1_{TBC\text{-}R343K}$. Error bars indicate mean and s.e.m.; data from three independent experiments were binned into 2-min intervals. (**c**) Regulated cycle of tethering and detethering. Vps21-mediated liposome tethering, measured by QLS, was examined during sequential addition of 20 μM GTP, 5 μM Vps9 and 10 μM $Gyp1_{TBC}$. Data are representative of three independent experiments. (**d**) Histograms of Vps21-decorated liposome size distributions, derived from QLS, at time points indicated in **c**. (**e**) TEM images of negatively stained samples withdrawn at indicated time points from experiment analyzed in **c**,**d**.

inactive mutant[43] $Gyp1_{TBC\text{-}R343K}$ had no effect on tethering even when added at 10 μM. GTP hydrolysis is therefore essential for the $Gyp1_{TBC}$-mediated disassembly of Vps21-GTP-mediated tethers (**Fig. 7b**).

Finally, in sequential-addition experiments, we reconstituted a complete cycle of regulated tethering and detethering (**Fig. 7c–e**). Liposomes decorated with Vps21-GDP were monitored by QLS (**Fig. 7c**). Addition of GTP alone had no effect, but subsequent Vps9 addition initiated an immediate and steady increase in tethering. Addition of $Gyp1_{TBC}$ rapidly reversed Vps9-stimulated tethering. QLS-derived particle size distributions (**Fig. 7d**) and TEM analysis of aliquots taken from the same reactions (**Fig. 7e**) verified that Vps9 and $Gyp1_{TBC}$ can drive complete cycles of tethering and detethering. Thus, Vps21-mediated tethering without effectors is Rab-selective, regulated by GTP, completely reversible and strictly controlled by upstream regulators.

DISCUSSION

Small G proteins orchestrate many biological processes, generally by acting through specialized effectors. Nevertheless, some small G proteins have intrinsic capabilities that complement or enhance the activities of their effectors. In vesicle formation, for example, activated Arf1 and Sar1 recruit the COPI and COPII coat complexes. However, the N-terminal domains of these small G proteins also interact directly with membranes to generate positive membrane curvature[44,45]. Here we have shown that like Arf1 and Sar1, Vps21 and some other yeast endosomal Rab proteins have both intrinsic and effector-mediated capabilities: they can dimerize or oligomerize in *trans* to tether membranes in a stringently GTP-dependent, tightly regulated and fully reversible reaction. In our working model, this intrinsic tethering

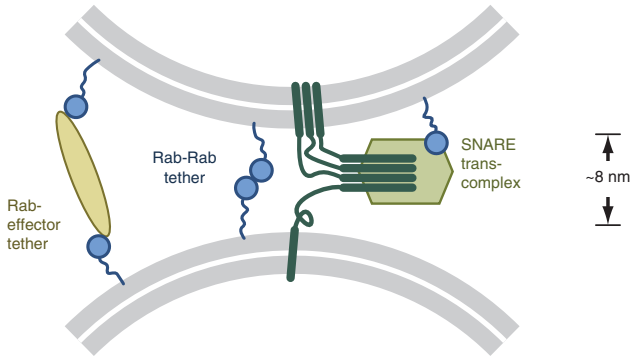

Figure 8 Model for Rab-Rab driven tethering in endosome docking and fusion. In this working model, three representative Rab functions are shown: classical effector-mediated tethering, Rab-Rab tethering and coordination of *trans*-SNARE complex assembly by a Rab-mediated recruitment of a SNARE-binding regulator. Together, these mechanisms could in principle coordinate an ordered tethering, docking and fusion sequence.

mechanism would cooperate with classical Rab-effector mechanisms to promote membrane tethering, docking and fusion (**Fig. 8**).

There are previous reports of Rab-Rab interactions. Rab5a, Rab5b and Rab5c, the closest mammalian orthologs of Vps21, have been detected in homotypic and heterotypic dimers by yeast two-hybrid assay, and Rab5b dimerizes *in vitro* and *in vivo* in an apparently GTP-dependent manner[38]. Moreover, in structural studies, the GDP-bound forms of Rab9 and Rab11a form crystallographic dimers[46–48]. So far, all Rabs reported to dimerize operate within endocytic trafficking pathways. These interactions are consistent with our results for yeast endocytic Rabs, raising the possibility that dimerization of endocytic Rabs is a general theme. The potential for complex regulation of tethering through Rab-Rab interactions is underscored by our identification of Rab pairs that show heterotypic interactions in yeast two-hybrid experiments and by our demonstration that a subset of these Rab pairs mediates heterotypic tethering in the liposome-bead assay. Similarly, Arf1, another small G protein, dimerizes during vesicle formation[49]. However, Arf1 does not mediate membrane tethering except in the presence of an effector[18]. Dimerization of Arf1 therefore seems restricted to *cis* rather than *trans* interactions.

Our biochemical and biophysical results demonstrate that Vps21 and some other endosomal Rabs have an intrinsic ability to tether membranes *in vitro*. Nevertheless, questions about the detailed mechanism of this tethering activity and its biological consequences remain. Although our results indicate that Vps21-Vps21 interactions are involved in tethering, we have so far not detected Vps21 dimerization or oligomerization in solution-phase assays using techniques including size-exclusion chromatography and multiangle light scattering. These findings raise the possibility that Vps21 dimerization is augmented by uncharacterized interactions between Vps21-GTP and the membrane. A requirement for both protein-protein and protein-membrane interactions in GTP-triggered tethering would be reminiscent of the requirement for interactions between synaptotagmin and SNARE proteins, and between synaptotagmin and lipids, in Ca^{2+}-riggered fusion[50].

The relative *in vivo* contributions to yeast endosome tethering by intrinsic Vps21 activity and by more conventional Vps21-effector mechanisms are not yet characterized, and they remain to be analyzed *in vivo*. Such experiments will require the isolation of Vps21 mutants that interact with the normal complement of Rab chaperones, upstream regulators and effectors, but which lack intrinsic tethering capacity. We are currently conducting genetic screens to identify and characterize mutant alleles with these properties.

If Rabs recruit specialized effectors, some of which are tethers, what is the function of Rab-Rab tethering? We suggest two possibilities. First, there is some redundancy among Rabs and effectors. For example, the yeast protein Vps8 is the only effector of Vps21 currently known to promote tethering *in vivo*. Vps8 is also needed for biosynthetic trafficking of carboxypeptidase Y to the vacuole. Notably, however, functional defects caused by Vps8 deletion are efficiently suppressed by Vps21 overproduction[24]. Conversely, Vps8 overexpression without Vps21 does not seem to mediate tethering[26]. These results support working models in which Vps8 and Vps21 normally act in concert, whereas without Vps8, an elevated level of secondary Vps21-mediated tethering is sufficient to support endolysosomal traffic. This secondary tethering activity could be mediated by Vps21-Vps21 interactions, by Vps21 interactions with another effector, or by some combination of these activities.

A second possible function for Rab-Rab tethering is suggested by the fact that Rab-Rab tethers probably operate at shorter range than classical effector-based tethers. Known and presumed tethers often assume extended structures that are presumed to allow vesicle capture and tethering over substantial distances (tens of nanometers). By contrast, Rab-Rab tethering must occur over shorter distances. Most Rabs attach to the membrane through a ~35-residue C-terminal disordered linker, which is doubly prenylated at its end. Our results show that the Vps21 linker is not needed for tethering (**Fig. 4**), but it probably influences the distance between tethered membranes. Because disordered polypeptides act as Brownian springs, Rabs probably interact in *trans* between membranes separated by ≤10 nm (**Fig. 8** and **Supplementary Methods**). Similarly, kinetically stable *trans*-SNARE complexes assemble only once docked membranes approach to within ~8 nm (refs. 51,52), raising the possibility of a 'handoff' mechanism whereby effector-mediated tethers promote Rab-Rab tethering, which, in turn, stably hold the membranes close enough to promote the initiation of SNARE zippering and fusion (**Fig. 8**). In the cases of Rab5 and Vps21, SNARE pairing is regulated by Vps45, a Sec1-Munc18 family protein recruited to the fusion site by Rab5 effector rabenosyn-5 or its yeast ortholog Vac1 (refs. 22,23,53,54). Finally, we speculate that Rab-Rab tethering might have emerged early in eukaryotic evolution, preceding more complex systems in which effectors contributed additional capabilities, including coordination of multiple small G proteins[2,55], tethering over longer distances[56], coupling of Rab activation to vesicle coat dynamics[57] and *trans*-SNARE complex assembly and membrane fusion[21,52,58].

METHODS

Methods and any associated references are available in the online version of the paper at http://www.nature.com/nsmb/.

Note: Supplementary information is available on the Nature Structural & Molecular Biology website.

ACKNOWLEDGMENTS

We thank P. Brennwald and J. Taraska for helpful discussion and D. Baker and R. Koga for assistance with multiangle light scattering experiments. High-throughput screening and support of M.V. was through the Yeast Resource Center (US National Institutes of Health (NIH) P41 RR11823). S.L. was supported in part by University of Washington Nanotechnology Integrative Graduate Education and Research Traineeship award (US National Science Foundation DGE-0504573). We thank the Murdock Charitable Trust and the Washington Research Foundation for generous support of our electron cryomicroscopy laboratory. T.G. was a Howard Hughes Medical Institute early career scientist and S.F. is a Howard Hughes Medical Institute investigator. This work was supported by NIH grant GM077349 and research scholar grant 10-026-01-CSM from the American Cancer Society.

AUTHOR CONTRIBUTIONS

S.Y.L. and A.J.M. conceived the project. S.Y.L. developed and validated the QLS-based tethering system; expressed, purified and characterized proteins; prepared liposomes and carried out and interpreted all QLS tethering experiments. C.L.B. and A.J.M. conceived and C.L.B. and S.Y.L. implemented the fluorescence microscopy-based tethering assays. T.G. did the E M. S.F. and M.V. developed the high-throughput yeast two-hybrid technology, and R.L.P. and M.V. executed and interpreted yeast two-hybrid screens and assays. S.Y.L. and A.J.M. wrote the paper.

COMPETING FINANCIAL INTERESTS

The authors declare no competing financial interests.

Published online at http://www.nature.com/nsmb/.
Reprints and permissions information is available online at http://www.nature.com/reprints/index.html.

1. Kornmann, B. *et al.* An ER-mitochondria tethering complex revealed by a synthetic biology screen. *Science* **325**, 477–481 (2009).
2. Grosshans, B.L., Ortiz, D. & Novick, P. Rabs and their effectors: achieving specificity in membrane traffic. *Proc. Natl. Acad. Sci. USA* **103**, 11821–11827 (2006).
3. Barr, F.A. Rab GTPase function in Golgi trafficking. *Semin. Cell Dev. Biol.* **20**, 780–783 (2009).
4. Singer-Kruger, B. *et al.* Role of three Rab5-like GTPases, Ypt51p, Ypt52p, and Ypt53p, in the endocytic and vacuolar protein sorting pathways of yeast. *J. Cell Biol.* **125**, 283–298 (1994).

5. Horazdovsky, B.F., Busch, G.R. & Emr, S.D. *VPS21* encodes a Rab5-like GTP binding protein that is required for the sorting of yeast vacuolar proteins. *EMBO J.* **13**, 1297–1309 (1994).
6. Gerrard, S.R., Bryant, N.J. & Stevens, T.H. *VPS21* controls entry of endocytosed and biosynthetic proteins into the yeast prevacuolar compartment. *Mol. Biol. Cell* **11**, 613–626 (2000).
7. Gorvel, J.P., Chavrier, P., Zerial, M. & Gruenberg, J. Rab5 controls early endosome fusion *in vitro*. *Cell* **64**, 915–925 (1991).
8. Bucci, C. *et al.* Co-operative regulation of endocytosis by three Rab5 isoforms. *FEBS Lett.* **366**, 65–71 (1995).
9. Barbieri, M.A. *et al.* Evidence for a symmetrical requirement for Rab5-GTP in *in vitro* endosome-endosome fusion. *J. Biol. Chem.* **273**, 25850–25855 (1998).
10. Simonsen, A. *et al.* EEA1 links PI(3)K function to Rab5 regulation of endosome fusion. *Nature* **394**, 494–498 (1998).
11. Christoforidis, S., McBride, H.M., Burgoyne, R.D. & Zerial, M. The Rab5 effector EEA1 is a core component of endosome docking. *Nature* **397**, 621–625 (1999).
12. Christoforidis, S. *et al.* Phosphatidylinositol-3-OH kinases are Rab5 effectors. *Nat. Cell Biol.* **1**, 249–252 (1999).
13. Lawe, D.C. *et al.* Sequential roles for phosphatidylinositol 3-phosphate and Rab5 in tethering and fusion of early endosomes via their interaction with EEA1. *J. Biol. Chem.* **277**, 8611–8617 (2002).
14. Davie, E.W. A brief historical review of the waterfall/cascade of blood coagulation. *J. Biol. Chem.* **278**, 50819–50832 (2003).
15. Weber, T. *et al.* SNAREpins: minimal machinery for membrane fusion. *Cell* **92**, 759–772 (1998).
16. Antonny, B., Madden, D., Hamamoto, S., Orci, L. & Schekman, R. Dynamics of the COPII coat with GTP and stable analogues. *Nat. Cell Biol.* **3**, 531–537 (2001).
17. Wollert, T. & Hurley, J.H. Molecular mechanism of multivesicular body biogenesis by ESCRT complexes. *Nature* **464**, 864–869 (2010).
18. Drin, G., Morello, V., Casella, J.F., Gounon, P. & Antonny, B. Asymmetric tethering of flat and curved lipid membranes by a golgin. *Science* **320**, 670–673 (2008).
19. Hickey, C.M. & Wickner, W. HOPS initiates vacuole docking by tethering membranes prior to trans-SNARE complex assembly. *Mol. Biol. Cell* **21**, 2297–2305 (2010).
20. Hickey, C.M., Stroupe, C. & Wickner, W. The major role of the Rab Ypt7p in vacuole fusion is supporting HOPS membrane association. *J. Biol. Chem.* **284**, 16118–16125 (2009).
21. Stroupe, C., Hickey, C.M., Mima, J., Burfeind, A.S. & Wickner, W. Minimal membrane docking requirements revealed by reconstitution of Rab GTPase-dependent membrane fusion from purified components. *Proc. Natl. Acad. Sci. USA* **106**, 17626–17633 (2009).
22. Peterson, M.R., Burd, C.G. & Emr, S.D. Vac1p coordinates Rab and phosphatidylinositol 3-kinase signaling in Vps45p-dependent vesicle docking/fusion at the endosome. *Curr. Biol.* **9**, 159–162 (1999).
23. Tall, G.G., Hama, H., DeWald, D.B. & Horazdovsky, B.F. The phosphatidylinositol 3-phosphate binding protein Vac1p interacts with a Rab GTPase and a Sec1p homologue to facilitate vesicle-mediated vacuolar protein sorting. *Mol. Biol. Cell* **10**, 1873–1889 (1999).
24. Horazdovsky, B.F., Cowles, C.R., Mustol, P., Holmes, M. & Emr, S.D. A novel RING finger protein, Vps8p, functionally interacts with the small GTPase, Vps21p, to facilitate soluble vacuolar protein localization. *J. Biol. Chem.* **271**, 33607–33615 (1996).
25. Peplowska, K., Markgraf, D.F., Ostrowicz, C.W., Bange, G. & Ungermann, C. The CORVET tethering complex interacts with the yeast Rab5 homolog Vps21 and is involved in endo-lysosomal biogenesis. *Dev. Cell* **12**, 739–750 (2007).
26. Markgraf, D.F. *et al.* The CORVET subunit Vps8 cooperates with the Rab5 homolog Vps21 to induce clustering of late endosomal compartments. *Mol. Biol. Cell* **20**, 5276–5289 (2009).
27. Plemel, R.L. *et al.* Subunit organization and Rab interactions of Vps-C protein complexes that control endolysosomal membrane traffic. *Mol. Biol. Cell* **22**, 1353–1363 (2011).
28. Gureasko, J. *et al.* Membrane-dependent signal integration by the Ras activator Son of sevenless. *Nat. Struct. Mol. Biol.* **15**, 452–461 (2008).
29. Hochuli, E., Dobeli, H. & Schacher, A. New metal chelate adsorbent selective for proteins and peptides containing neighbouring histidine residues. *J. Chromatogr. A* **411**, 177–184 (1987).
30. Wang, L., Seeley, E.S., Wickner, W. & Merz, A.J. Vacuole fusion at a ring of vertex docking sites leaves membrane fragments within the organelle. *Cell* **108**, 357–369 (2002).
31. Ghaemmaghami, S. *et al.* Global analysis of protein expression in yeast. *Nature* **425**, 737–741 (2003).
32. Takamori, S. *et al.* Molecular anatomy of a trafficking organelle. *Cell* **127**, 831–846 (2006).
33. Patel, S.S. & Rexach, M.F. Discovering novel interactions at the nuclear pore complex using bead halo: a rapid method for detecting molecular interactions of high and low affinity at equilibrium. *Mol. Cell. Proteomics* **7**, 121–131 (2008).
34. Braun, P. *et al.* An experimentally derived confidence score for binary protein-protein interactions. *Nat. Methods* **6**, 91–97 (2009).
35. Chen, Y.C., Rajagopala, S.V., Stellberger, T. & Uetz, P. Exhaustive benchmarking of the yeast two-hybrid system. *Nat. Methods* **7**, 667–668 author reply 668 (2010).
36. Brett, C.L. *et al.* Efficient termination of vacuolar Rab GTPase signaling requires coordinated action by a GAP and a protein kinase. *J. Cell Biol.* **182**, 1141–1151 (2008).
37. Ho, Y. *et al.* Systematic identification of protein complexes in *Saccharomyces cerevisiae* by mass spectrometry. *Nature* **415**, 180–183 (2002).
38. Daitoku, H., Isida, J., Fujiwara, K., Nakajima, T. & Fukamizu, A. Dimerization of small GTPase Rab5. *Int. J. Mol. Med.* **8**, 397–404 (2001).
39. Pawelec, A., Arsic, J. & Kolling, R. Mapping of Vps21 and HOPS binding sites in Vps8 and effect of binding site mutants on endocytic trafficking. *Eukaryot. Cell* **9**, 602–610 (2010).
40. Hama, H., Tall, G.G. & Horazdovsky, B.F. Vps9p is a guanine nucleotide exchange factor involved in vesicle-mediated vacuolar protein transport. *J. Biol. Chem.* **274**, 15284–15291 (1999).
41. Buvelot Frei, S. *et al.* Bioinformatic and comparative localization of Rab proteins reveals functional insights into the uncharacterized GTPases Ypt10p and Ypt11p. *Mol. Cell. Biol.* **26**, 7299–7317 (2006).
42. Du, L.L., Collins, R.N. & Novick, P.J. Identification of a Sec4p GTPase-activating protein (GAP) as a novel member of a Rab GAP family. *J. Biol. Chem.* **273**, 3253–3256 (1998).
43. Pan, X., Eathiraj, S., Munson, M. & Lambright, D.G. TBC-domain GAPs for Rab GTPases accelerate GTP hydrolysis by a dual-finger mechanism. *Nature* **442**, 303–306 (2006).
44. Lee, M.C. *et al.* Sar1p N-terminal helix initiates membrane curvature and completes the fission of a COPII vesicle. *Cell* **122**, 605–617 (2005).
45. Pucadyil, T.J. & Schmid, S.L. Conserved functions of membrane active GTPases in coated vesicle formation. *Science* **325**, 1217–1220 (2009).
46. Wittmann, J.G. & Rudolph, M.G. Crystal structure of Rab9 complexed to GDP reveals a dimer with an active conformation of switch II. *FEBS Lett.* **568**, 23–29 (2004).
47. Pasqualato, S. *et al.* The structural GDP/GTP cycle of Rab11 reveals a novel interface involved in the dynamics of recycling endosomes. *J. Biol. Chem.* **279**, 11480–11488 (2004).
48. Scapin, S.M. *et al.* The crystal structure of the small GTPase Rab11b reveals critical differences relative to the Rab11a isoform. *J. Struct. Biol.* **154**, 260–268 (2006).
49. Beck, R. *et al.* Membrane curvature induced by Arf1-GTP is essential for vesicle formation. *Proc. Natl. Acad. Sci. USA* **105**, 11731–11736 (2008).
50. Chapman, E.R. How does synaptotagmin trigger neurotransmitter release? *Annu. Rev. Biochem.* **77**, 615–641 (2008).
51. Li, F. *et al.* Energetics and dynamics of SNAREpin folding across lipid bilayers. *Nat. Struct. Mol. Biol.* **14**, 890–896 (2007).
52. Schwartz, M.L. & Merz, A.J. Capture and release of partially zipped trans-SNARE complexes on intact organelles. *J. Cell Biol.* **185**, 535–549 (2009).
53. Nielsen, E. *et al.* Rabenosyn-5, a novel Rab5 effector, is complexed with hVPS45 and recruited to endosomes through a FYVE finger domain. *J. Cell Biol.* **151**, 601–612 (2000).
54. Furgason, M.L. *et al.* The N-terminal peptide of the syntaxin Tlg2p modulates binding of its closed conformation to Vps45p. *Proc. Natl. Acad. Sci. USA* **106**, 14303–14308 (2009).
55. Sinka, R., Gillingham, A.K., Kondylis, V. & Munro, S. Golgi coiled-coil proteins contain multiple binding sites for Rab family G proteins. *J. Cell Biol.* **183**, 607–615 (2008).
56. Hayes, G.L. *et al.* Multiple Rab GTPase binding sites in GCC185 suggest a model for vesicle tethering at the trans-Golgi. *Mol. Biol. Cell* **20**, 209–217 (2009).
57. Angers, C.G. & Merz, A.J. New links between vesicle coats and Rab-mediated vesicle targeting. *Semin. Cell Dev. Biol.* **22**, 18–26 (2011).
58. Ohya, T. *et al.* Reconstitution of Rab- and SNARE-dependent membrane fusion by synthetic endosomes. *Nature* **459**, 1091–1097 (2009).

ONLINE METHODS

Proteins. See **Supplementary Methods** for detailed descriptions of protein expression construct, expression and purification.

Liposomes. A 2.5-mg quantity of lipids consisting of egg phosphatidylcholine (PC) and Ni^{2+}-NTA-DOGS dissolved in chloroform (Avanti Polar Lipids) were mixed, dried under an argon stream and placed under vacuum overnight. For assays requiring fluorescent liposomes, 0.4 mol% Texas Red DPPE (Invitrogen) was incorporated into the lipid mixture. Lipid films were hydrated in liposome reaction buffer (20 mM HEPES-NaOH, pH 7.5, 150 mM NaCl, 1 mM $MgCl_2$ and 2 mM 2-mercaptoethanol) to 2.5 mg ml^{-1} before extrusion through a 0.1 μm polycarbonate filter (Avanti Polar Lipids). To change the ionic strength of the liposome environment, liposomes were prepared in liposome reaction buffer at the indicated NaCl concentrations.

Quasielastic light scattering tethering assay. In general, samples were prepared by incubating 100 μl of liposomes with 20 μl nucleotide-loaded Rab-His_{10} at 24.5 °C for 1 h, then diluted to 1 ml for QLS measurement. See **Supplementary Methods** for detailed information on QLS. Nucleotide-loaded Rab-His_{10} protein was prepared by incubating 4–5 mg ml^{-1} Rab-His_{10} with a 30-fold molar excess of guanine nucleotide and 5 mM EDTA for 1 h at 25–27 °C in 20 mM HEPES-NaOH, pH 7.5, 150 mM NaCl and 1 mM DTT. Nucleotide exchange was terminated with 10 mM $MgCl_2$ on ice for 15 min and free nucleotide was removed by size exclusion using a Micro Bio-Spin column (Bio-Rad) pre-equilibrated with liposome reaction buffer at the indicated NaCl concentration.

Rab membrane density was altered by incubating liposomes at varying Rab to Ni^{2+}-NTA-DOGS molar ratios (**Supplementary Table 4**). Except as indicated, liposomes contained 4.5 mol% Ni^{2+}-NTA-DOGS and were incubated with 20 μl of Rab-His_{10} at a molar ratio of 0.067:1 Rab/Ni^{2+}-NTA-DOGS, yielding a surface density of ≤3,750 Vps21-His_{10} μm^{-2}. For GEF experiments, Vps9 was added to 200 μl of liposomes preincubated with GDP-bound Vps21-His_{10} and diluted to 640 μl for QLS measurement. GTP (10 μl) was added to initiate tethering. For GAP experiments, 200 μl of liposomes preincubated with GTP-loaded Vps21-His_{10} was diluted to 550 μl for QLS measurement. $Gyp1_{TBC}$ or $Gyp1_{TBC\text{-}R343K}$ (100 μl) was added to initiate disassembly of liposome clusters. For the reconstitution of a full tethering cycle, 400 μl liposomes were preincubated with GDP-bound Vps21-His_{10}. The mixture was diluted to 640 μl for QLS measurements, and GTP, Vps9 and $Gyp1_{TBC}$ were subsequently added, in order, to final volumes of 650 μl, 700 μl and 850 μl. The concentrations of GTP, Vps9 and $Gyp1_{TBC}$ were maintained at 20 μM, 5 μM and 10 μM, respectively, throughout the sequential-addition experiment.

Fluorescent tethering assay and bead-liposome tethering assay. GST-Rab-coupled glutathione–Sepharose 4B beads (GE Healthcare) were prepared as described[27,36] except that an equal volume of *Escherichia coli* lysate expressing untagged $Gyp1_{TBC}$ was mixed with the Rab-expressing cell lysate to drive Rab conversion into the GDP-bound state. Nucleotide loading of Rabs was done by incubating GST-Rab beads in loading buffer (50 mM HEPES-NaOH, pH 7.8, 100 mM NaCl, 5 mM 2-mercaptoethanol, 5 mM EDTA and 500 μM guanine nucleotide) for 1 h at 24.5 °C. An equal volume of quenching buffer (50 mM HEPES-NaOH, pH 7.8, 100 mM NaCl, 5 mM 2-mercaptoethanol and 10 mM $MgCl_2$) was then added to each reaction and incubated for an additional 15 min. Nucleotide-loaded GST-Rab beads were then washed twice with reaction buffer (20 mM HEPES-NaOH, pH 7.4, 125 mM NaCl, 5 mM 2-mercaptoethanol and 5 mM $MgCl_2$). Fluorescent liposome tethering reactions or bead-liposome tethering reactions were prepared on ice by mixing 50 μl reaction buffer and 40 μl fluorescent liposome suspension with or without 50 μl of packed, nucleotide-loaded GST-Rab beads. Nucleotide-loaded Rab-His_{10} (6 μg) was then added to initiate tethering. The upper-bound density of Vps21-His_{10} on liposomes used for the bead assay was ≤4,700 Vps21-His_{10} μm^{-2}. Reactions were brought to 24.5 °C, incubated for 20, 40 or 60 min, then imaged.

Micrographs were acquired using a microscope (IX71; Olympus) equipped with an electron-multiplying charge-coupled device (iXon; Andor). Epifluorescence illumination was done by green and blue light-emitting diodes (>350-mW output) coupled to the microscope's back aperture by a multimode optical fiber and driven by custom electronics. Objective lenses were UPlanApo (0.40 numerical aperture (NA), 10×) or PlanApoN (1.45 NA, 60×). The microscope and camera were driven by iQ software (version 6.0.3.62; Andor), and micrographs were processed using ImageJ (version 1.36b; NIH) and Photoshop (version 8.0; Adobe). For display, images were sharpened by applying unsharp masking.

Electron microscopy. For negative-stain EM, samples were stained with 0.75% (w/v) uranyl formate. Images were collected using a 100 kV transmission electron microscope (Morgagni M268, FEI) equipped with a Gatan bottom mount 4k × 2k charge-coupled device camera. Images were recorded at either 4,400× or 8,900× magnification at the specimen level.

Yeast two-hybrid assays. Genome-wide two-hybrid analysis was done as described[13] in collaboration with the University of Washington Yeast Resource Center. Parent strains and plasmids were obtained from the Yeast Resource Center. Two-hybrid constructs were cloned individually into haploid tester strains using gap repair and homologous recombination. Prey domains were cloned into the plasmid pOAD and transformed into the yeast strain PJ69-4a. Bait domains were cloned into pOBD2 and transformed into PJ69-4α. Clonal isolates were obtained and verified by PCR. Sequencing was done using dideoxy chain termination.

Focused interaction tests were done by mating bait and prey haploid strains in 96-well plates, which were then pinned to YPD plates supplemented with adenine using a 48-spoke inoculating manifold. The mating plates were grown at 30 °C overnight before selecting diploids by replica plating onto medium supplemented with adenine but lacking tryptophan and leucine. Diploid colonies were grown at 30 °C for 2 d, then replica plated to medium supplemented with adenine and 1.5 mM 3-amino-1,2,4-triazole but lacking tryptophan, leucine and histidine. Plates were scored for growth after 5 d at 30 °C.

Intrinsic tethering activity of endosomal Rab proteins

Sheng-Ying Lo, Christopher L. Brett, Rachael L. Plemel, Marissa Vignali, Stanley Fields, Tamir Gonen, and Alexey J. Merz

Please address correspondence to Alex Merz:
merza@uw.edu · www.merzlab.org

Supplementary Information:

- **Supplementary Figures 1-4**
- **Supplementary Tables 1-4**
- **Supplementary Methods**
- **References**

Nature Structural & Molecular Biology: doi:10.1038/nsmb.2162

Supplementary Figure 1

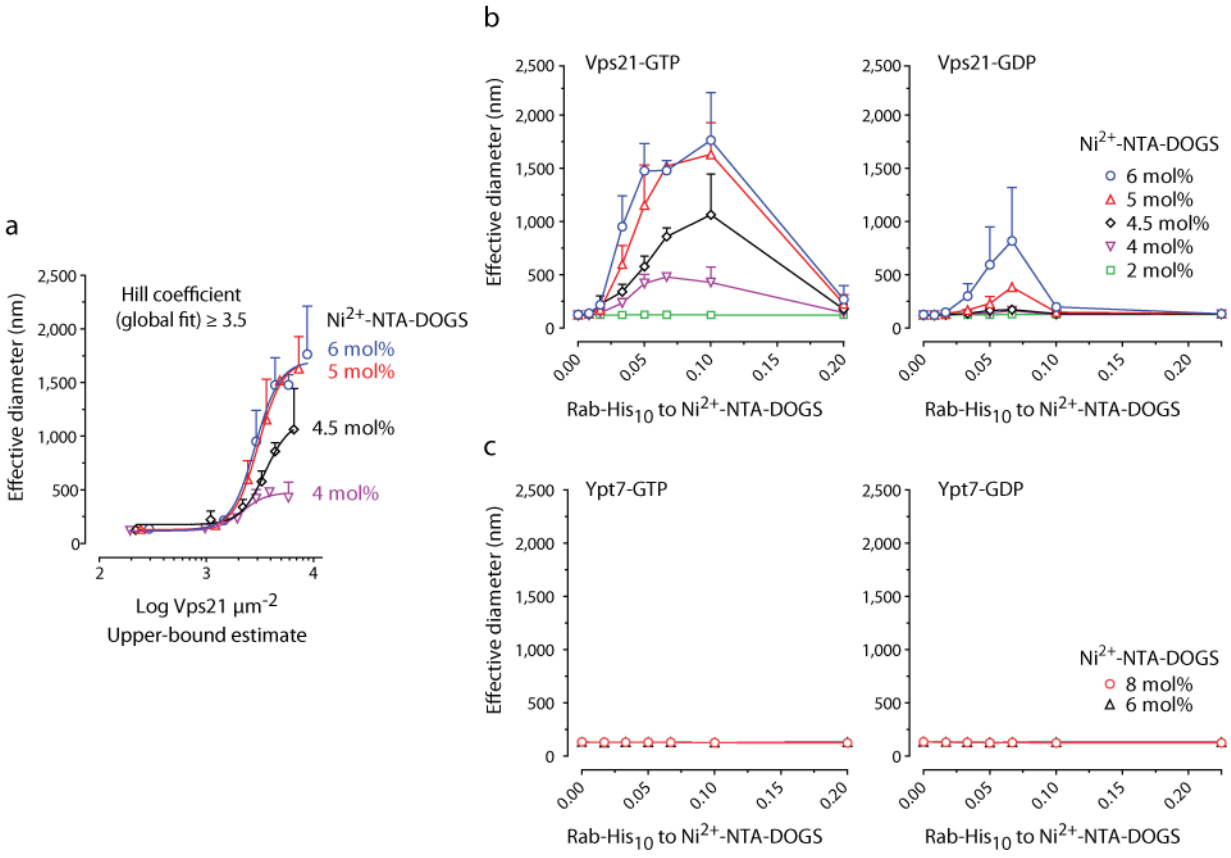

Supplementary Figure 1. Titration of Vps21 and Ypt7 in tethering reactions.
(a) Liposome tethering, measured by QLS, was examined as a function of Vps21-GTP membrane surface density (log scale; mean ± s.e.m.). Lines show fits of the Hill equation to the same data shown in Fig. 2. The Hill coefficient was fit as a single global variable. Allowing the Hill coefficient to vary locally did not substantially improve the fit. The Vps21 density was estimated as shown in Supplementary Table 4. **(b and c)** Liposome tethering was measured by QLS after incubating different mol% Ni^{2+}-NTA-DOGS liposomes at various ratios of Rab to outer-leaflet Ni^{2+}-NTA-DOGS for 60 minutes (mean ± s.e.m). Data for Vps21-decorated liposome tethering curves were collected from three independent experiments except for the 0.067 and 0.0083 Rab to Ni^{2+}-NTA-DOGS data points. Data for Ypt7-decorated liposome tethering curves were collected from a single experiment. Across several experiments, Ypt7-decorated liposomes failed to tether even at high densities where Vps21 exhibited nucleotide-independent homotypic interactions.

Supplementary Figure 2

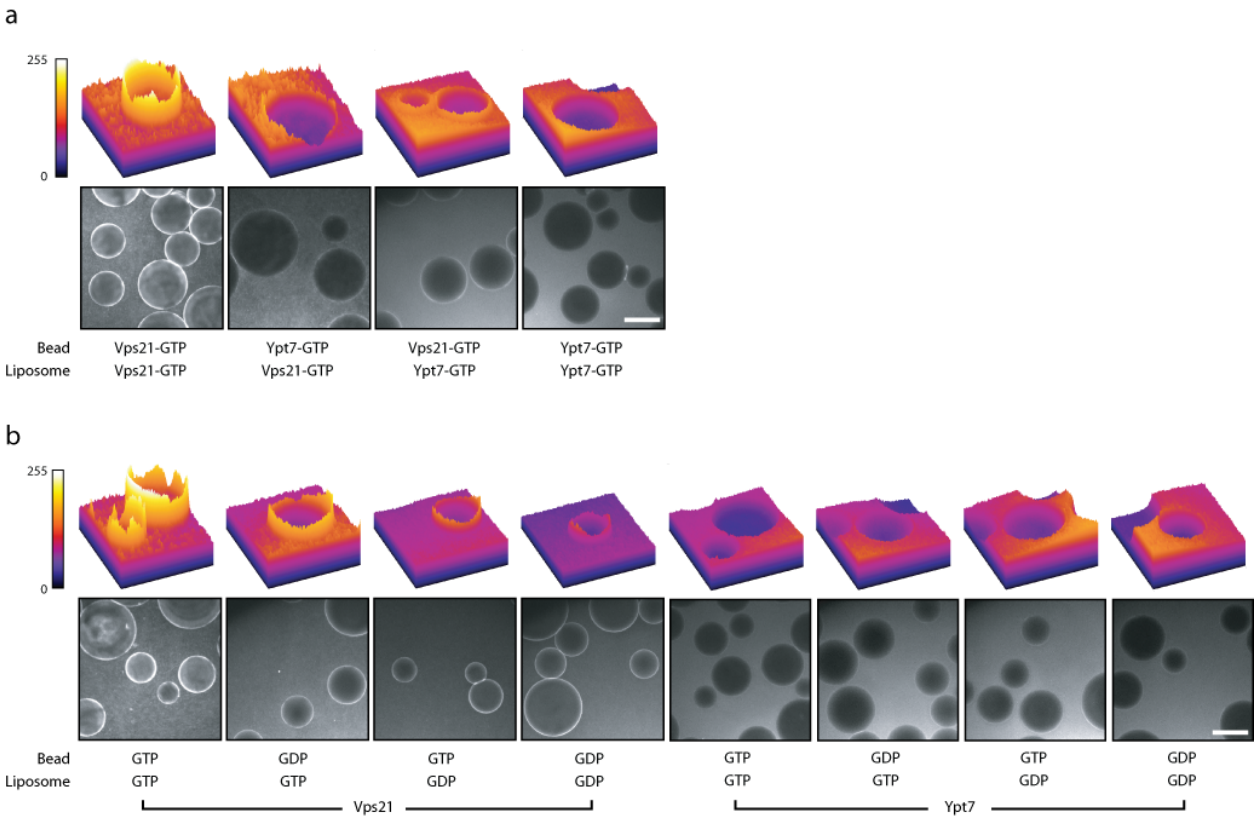

Supplementary Figure 2. Tethering requires symmetric *trans*-interactions of Vps21-GTP. **(a)** Assays were performed as in Fig. 3a, except that fluorescent liposomes were prepared with 4.5 mol% rather than 6 mol% Ni^{2+}-NTA-DOGS, and the Rabs on the beads or liposomes were either Ypt7 or Vps21, as indicated. The bottom panels in each set show representative fields of beads under epifluorescence illumination. The top panels show fluorescence intensity profile plots of representative beads. **(b)** Assays were performed as in panel a, except that Rabs were loaded with either GDP or GTP, as indicated. Maximum fluorescence intensity surrounding glutathione–Sepharose 4B resins was observed only when GTP-loaded Vps21 was present on both the beads and the liposomes. Scale bars = 75 μm.

Nature Structural & Molecular Biology: doi:10.1038/nsmb.2162

Supplementary Figure 3

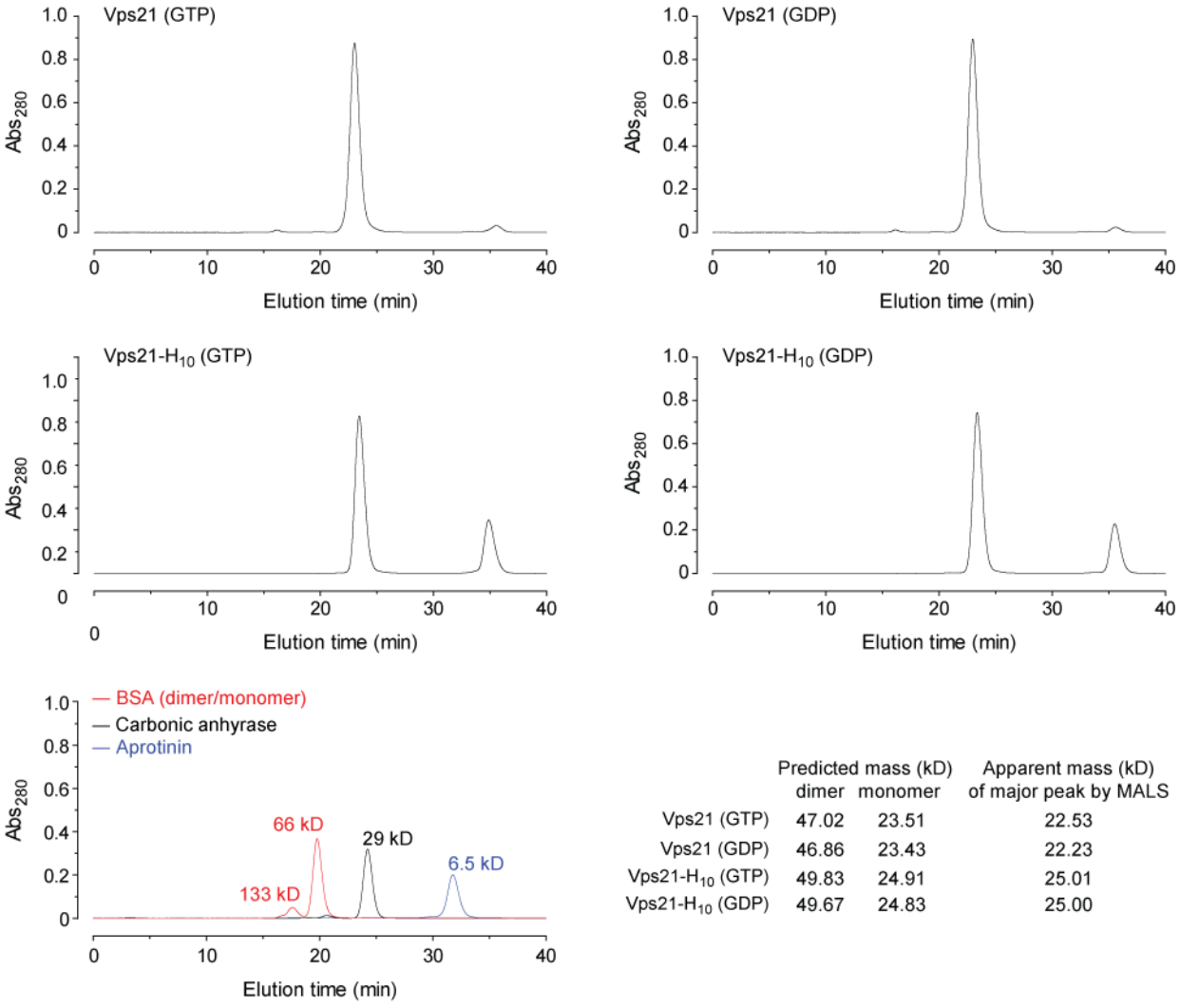

	Predicted mass (kD) dimer	monomer	Apparent mass (kD) of major peak by MALS
Vps21 (GTP)	47.02	23.51	22.53
Vps21 (GDP)	46.86	23.43	22.23
Vps21-H_{10} (GTP)	49.83	24.91	25.01
Vps21-H_{10} (GDP)	49.67	24.83	25.00

Supplementary Figure 3. Solution phase characterization of recombinant Vps21 preparations by analytical size exclusion chromatography (SEC) and multi-angle light scattering (MALS).
Plots show protein absorbance at 280 nm (Abs_{280}) versus elution time for Vps21 or Vps21-His_{10}, pre-loaded with GTP or GDP on a Superdex 75 10/300 GL column. MALS data obtained during the SEC run were analyzed with ASTRA software (Wyatt Technologies) to obtain the apparent molecular masses of species in the major absorbance peaks. The late-eluting minor absorbance peaks are presumed to correspond to free guanosine nucleotides. In experiments with mass standards, BSA dimer and monomer (M_W ~ 132.9 and 66.4 kDa) eluted at 17.4 and 19.7 min, carbonic anhydrase (M_W ~ 29 kDa) eluted at 24.1 min, and aprotinin (M_w ~ 6.5 kDa) eluted at 31.6 min.

Supplementary Figure 4

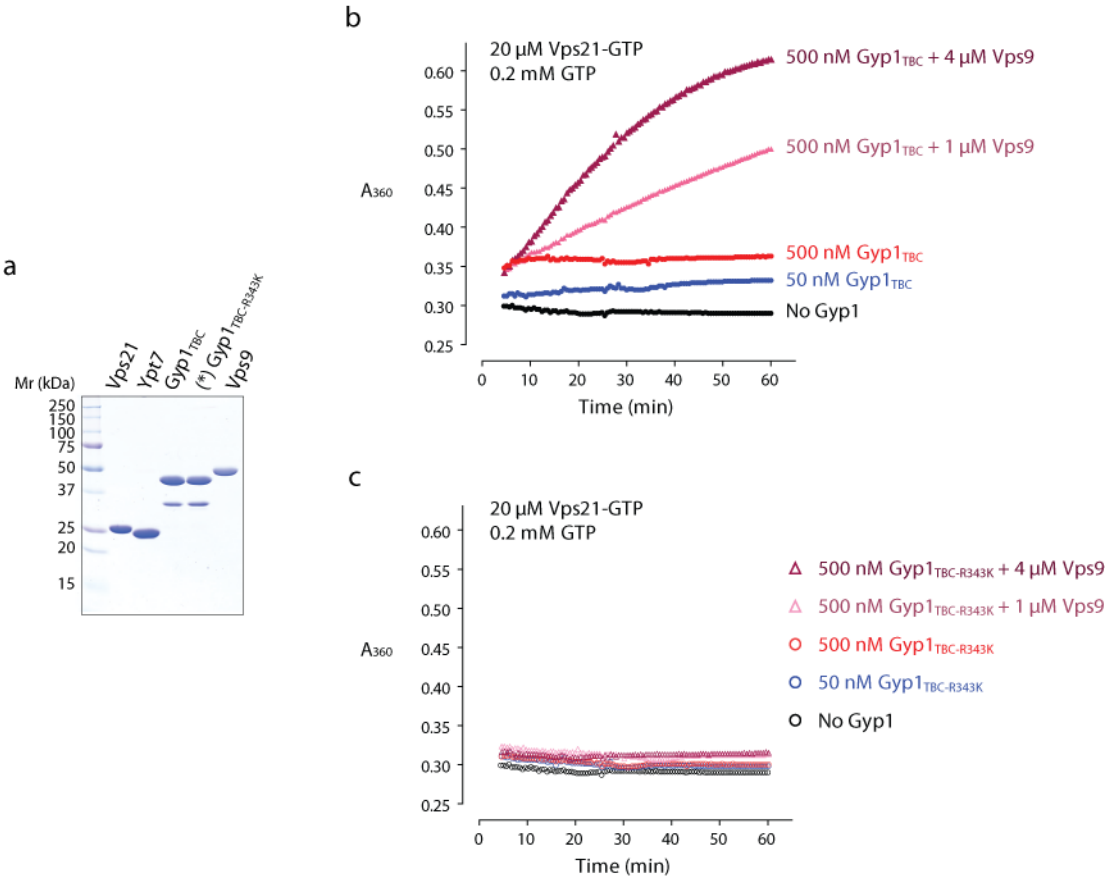

Supplementary Figure 4. Multiple cycles of Vps 21 GTP hydrolysis in the presence of $Gyp1_{TBC}$ and Vps9. **(a)** Purified proteins were separated by polyacrylamide gel electrophoresis (5 µg per lane) and stained with Coomassie brilliant blue. **(b)** Time course of solution-based GTP hydrolysis by Vps21 in the presence of the GAP $Gyp1_{TBC}$, with or without the GEF Vps9. $Gyp1_{TBC}$ alone triggered only a single round of GTP hydrolysis because spontaneous GDP release by Vps21 is extremely slow. In these single-round hydrolysis experiments (without Vps9), the maximum amount of inorganic phosphate released in response to $Gyp1_{TBC}$ addition was 10 µM (1 nmol in a 100 µl reaction containing 2 nmol of Vps21). This corresponds to GTP loading and hydrolysis on at least 50% of the input Vps21 molecules. The addition of Vps9 stimulated nucleotide exchange, allowing multiple rounds of GTP hydrolysis to occur on each Vps21 molecule in the presence of $Gyp1_{TBC}$. The data shown are representative of three independent experiments. **(c)** Assays were performed as in (b), except that $Gyp1_{TBC}$ was replaced by the catalytically inactive mutant $Gyp1_{TBC\text{-}R343K}$.

Supplementary Table 1

Partial results from high-throughput screens for Rab-interacting proteins. Two full replicate screens were run in parallel for each bait, and for each bait more than 5,000 preys were screened. A total of 340 hits were obtained from over 65,000 crosses. Only Rab-Rab and Rab-chaperone interactions are shown. Other hits will be presented elsewhere. The "hits" column indicates whether a given interaction was detected in one or both replicates. Ypt7 and Vps21 bait constructs marked "QL" are mutant forms that are predicted to be hyperactivated due to defective GTP hydrolysis ($Ypt7_{Q68L}$ and $Vps21_{Q66L}$). Note: For hits marked with an asterisk (*), positively-interacting clones were isolated, their prey plasmid inserts were sequenced, and the prey inserts were found to harbor point mutations. These include Ypt52(Y81H) and Ypt53 (G165D and V33I). See Table S2 for further Y2H analysis of these mutants.

Supplementary Table 2

Rab versus Rab interactions in pairwise Y2H tests. The prey constructs used for these assays were constructed independently of the arrayed preys used for high-throughput screens (Table S1), and all baits and preys shown in Table S2 were verified by DNA sequencing. Data in this table represent interaction scores from 0 (no interaction detected) to 3 (strong interaction). Each score represents the mean result from at least two independent assays. Empty cells indicate interactions not tested. In addition to Rabs, known Vps21 interactors were tested. Vps21-GTP can bind to at least three effectors: Pep7, and the CORVET subunits Vps3 and Vps8 (Refs. 1-3). Vps21-GDP interacts with the GEF Vps9 (Ref. 4).

Supplementary Table 3

Effects of nucleotide-bound state and prenylation on Vps21 self-interactions. Assays were performed and scored as for Table S2. Constructs denoted "LF" (lipid-free) were double mutants (C208S C210S) lacking C-terminal prenylation acceptor sites[5,6].

Supplementary Table 4

Concentrations and surface densities of Rab and Ni^{2+}-NTA-DOGS during tethering incubations for Fig. 2 and Supplementary Fig. 1.

Supplementary Table 1. Results of high-throughput screens for Rab-interacting proteins.

~Bait ORF	~Prey ORF	Hits	Notes
Rab chaperones			
Sec4	GDI1 (YER136W)	2	GDP dissociation inhibitor; universal Rab chaperone
Vps21	GDI1 (YER136W)	2	GDP dissociation inhibitor; universal Rab chaperone
Ypt1	GDI1 (YER136W)	2	GDP dissociation inhibitor; universal Rab chaperone
Ypt10	GDI1 (YER136W)	2	GDP dissociation inhibitor; universal Rab chaperone
Ypt31	GDI1 (YER136W)	2	GDP dissociation inhibitor; universal Rab chaperone
Ypt32	GDI1 (YER136W)	1	GDP dissociation inhibitor; universal Rab chaperone
Ypt52	GDI1 (YER136W)	2	GDP dissociation inhibitor; universal Rab chaperone
Ypt53	GDI1 (YER136W)	2	GDP dissociation inhibitor; universal Rab chaperone
Ypt6	GDI1 (YER136W)	2	GDP dissociation inhibitor; universal Rab chaperone
Ypt7	GDI1 (YER136W)	2	GDP dissociation inhibitor; universal Rab chaperone
Ypt7 QL	GDI1 (YER136W)	2	GDP dissociation inhibitor; universal Rab chaperone
Ypt7	MRS6 (YOR370C)	2	Rab escort protein
Ypt7 QL	MRS6 (YOR370C)	2	Rab escort protein
Vps21	YIF1 (YNL263C)	2	Putative GDI dissociation factor
Vps21 QL	YIF1 (YNL263C)	2	Putative GDI dissociation factor
Ypt1	YIF1 (YNL263C)	2	Putative GDI dissociation factor
Ypt52	YIF1 (YNL263C)	2	Putative GDI dissociation factor
Ypt53	YIF1 (YNL263C)	2	Putative GDI dissociation factor
Vps21	YIP1 (YGR172C)	2	Putative GDI dissociation factor
Vps21 QL	YIP1 (YGR172C)	2	Putative GDI dissociation factor
Ypt1	YIP1 (YGR172C)	2	Putative GDI dissociation factor
Ypt31	YIP1 (YGR172C)	2	Putative GDI dissociation factor
Ypt52	YIP1 (YGR172C)	2	Putative GDI dissociation factor
Ypt53	YIP1 (YGR172C)	2	Putative GDI dissociation factor
Ypt1	YIP4 (YGL198W)	1	Putative GDI dissociation factor
Ypt52	YIP4 (YGL198W)	2	Putative GDI dissociation factor
Ypt1	YIP5 (YGL161C)	2	Putative GDI dissociation factor
Ypt52	YIP5 (YGL161C)	2	Putative GDI dissociation factor
Rab-Rab			
Vps21	*VPS21 (YOR089C)*	1	Rab GTPase required for transport during endocytosis and for correct sorting of vacuolar hydrolases; localized in endocytic intermediates; detected in mitochondria; geranylgeranylation required for membrane association; mammalian Rab5 homolog
Vps21 QL	*VPS21 (YOR089C)*	2	Rab GTPase required for transport during endocytosis and for correct sorting of vacuolar hydrolases; localized in endocytic intermediates; detected in mitochondria; geranylgeranylation required for membrane association; mammalian Rab5 homolog
Vps21	*YPT52 (YKR014C)**	1	Rab GTPase, similar to Ypt51p and Ypt53p and to mammalian rab5; required for vacuolar protein sorting and endocytosis
Ypt52	*YPT52 (YKR014C)**	2	Rab GTPase, similar to Ypt51p and Ypt53p and to mammalian rab5; required for vacuolar protein sorting and endocytosis
Vps21	*YPT53 (YNL093W)**	2	Rab GTPase, similar to Ypt51p and Ypt52p and to mammalian rab5; required for vacuolar protein sorting and endocytosis
Vps21 QL	*YPT53 (YNL093W)**	2	Rab GTPase, similar to Ypt51p and Ypt52p and to mammalian rab5; required for vacuolar protein sorting and endocytosis
Ypt52	*YPT53 (YNL093W)**	2	Rab GTPase, similar to Ypt51p and Ypt52p and to mammalian rab5; required for vacuolar protein sorting and endocytosis
Ypt53	*YPT53 (YNL093W)**	2	Rab GTPase, similar to Ypt51p and Ypt52p and to mammalian rab5; required for vacuolar protein sorting and endocytosis
Ypt52	*YPT6 (YLR262C)*	2	Rab GTPase, Ras-like GTP binding protein involved in the secretory pathway, required for fusion of endosome-derived vesicles with the late Golgi, maturation of the vacuolar carboxypeptidase Y; has similarity to the human GTPase, Rab6
Ypt10	*YPT7 (YML001W)*	1	Rab GTPase; GTP-binding protein of the rab family; required for homotypic fusion event in vacuole inheritance, for endosome-endosome fusion, similar to mammalian Rab7

Supplementary Table 2: Rab vs. Rab interactions in pairwise Y2H tests

Bait \ Prey	Ypt1 wt	Sec4 wt	Ypt6 wt	Ypt10 wt	Ypt11 wt	Ypt31 wt	Ypt32 wt	Ypt7 wt	Ypt52 wt	Ypt52 (Y81H)	Ypt53 wt	Ypt53 (G165D)	Ypt53 (V33I)	Vps21 wt	Vps21-GTP (Q66L)	Vps21-GDP (S21L)	Gdi1 - Rab chaperone	Vps9 - Vps21 GEF
Ypt1 wt	0	0	0	0	0	0	0	0	0	0	0	0	0	0	0	0	·	0
Sec4 wt	0	0	0	0	0	0	0	0	0	0	0	0	0	0	0	0	·	0
Ypt6 wt	0	0	0	0	0	0	0	0	0	0	0	0	0	0	0	0	·	0
Ypt10 wt	0	0	1	0	0	0	0	3	0	0	0	0	0	1	1	0	·	0
Ypt11 wt	0	0	0	0	0	0	0	0	0	0	0	0	0	0	0	0	·	0
Ypt31 wt	0	0	0	0	0	0	0	0	0	0	0	0	0	0	0	0	·	0
Ypt32 wt	0	0	0	0	0	0	0	0	0	0	0	0	0	0	0	0	·	0
Ypt7 wt	0	0	0	0	0	0	0	2	0	0	0	0	0	0	0	0	·	0
Ypt52 wt	0	0	0	0	0	0	0	1	0	3	0	1	0	2	2	0	0	0
Ypt52 (Y81H)	0	0	1	0	0	0	0	0	0	3	0	1	0	2	1	0	0	0
Ypt53 wt	0	0	0	0	0	0	0	2	0	3	0	2	0	2	2	0	0	0
Ypt53 (G165D)	0	0	0	0	0	0	0	1	0	3	0	2	0	3	3	0	1	1
Ypt53 (V33I)	·	·	·	·	·	·	·	1	0	3	0	3	0	3	3	0	3	0
Vps21 wt	0	0	1	0	0	0	0	1	0	3	0	3	0	3	2	0	3	0
Vps21-GTP (Q66L)	0	0	0	0	0	0	0	3	0	3	0	3	0	3	3	0	2	0
Vps21-GDP (S21L)	0	0	0	0	0	0	0	0	0	0	0	0	0	0	0	0	0	3
Vps21 (R68A)	·	·	·	·	·	·	·	0	0	3	0	3	0	3	3	0	0	0
Vps21 (V28I)	·	·	·	·	·	·	·	0	0	3	0	2	0	3	2	0	3	0
Vps21 (V28K)	·	·	·	·	·	·	·	0	0	3	0	2	0	3	2	0	3	0
Vps21 (Y77A)	·	·	·	·	·	·	·	0	0	3	0	1	0	3	1	0	2	0
Vps21 (Y77H)	·	·	·	·	·	·	·	0	0	3	0	2	0	2	2	0	2	0
Vps21 (G157D)	·	·	·	·	·	·	·	0	0	3	0	2	0	3	2	0	3	0
Vps21 (G157F)	·	·	·	·	·	·	·	0	0	3	0	2	0	3	3	0	2	0
Pep7 effector	0	0	0	0	0	0	0	0	0	3	0	2	·	2	2	0	0	0
Vps3 (1-492) effector	0	0	0	0	0	0	0	0	0	2	0	2	·	2	2	0	0	0
Vps8 (422-1187) effector	0	0	0	0	0	0	0	0	0	3	0	3	·	3	3	0	0	0

Supplementary Table 3: Effects of nucleotide-bound state and C-terminal prenylation on Vps21 self-interaction in Y2H assays

Bait \ Prey	Vps21 wt LF	Vps21-GDP(S21L) LF	Vps21-GTP (Q66L) LF	Vps21 wt	Vps21-GDP (S21L)	Vps21-GTP (Q66L)
Vps21 wt LF	0	0	0	0	0	0
Vps21-GDP (S21L) LF	0	0	0	0	0	0
Vps21-GTP (Q66L) LF	0	0	0	0	0	0
Vps21 wt	1	1	0	3	0.5	2
Vps21-GDP (S21L)	0	0	0	0	0	0
Vps21-GTP (Q66L)	1	0	0	3	0	2.5

Supplementary Table 4

Concentrations of Rab and Ni^{2+}-NTA-DOGS during tethering incubations for Fig. 2 and Supplementary Fig. S1.

Calculated molar concentration of outer leaflet Ni^{2+}-NTA-DOGS (M):

2	4	4.5	5	6
3.26E-05	6.48E-05	7.27E-05	8.07E-05	9.64E-05

$$\text{Outer leaflet } Ni^{2+}\text{-NTA-DOGS (M)} = 2.5\ \frac{g}{L}\ \text{lipid} \times \frac{\text{mol\% } Ni^{2+}\text{-NTA-DOGS}}{760 \times \text{mol\% EggPC} + 1057 \times \text{mol\% } Ni^{2+}\text{-NTA-DOGS}} \times \frac{1}{2}$$

where FW of Egg PC=760 $\frac{g}{mol}$ and FW of Ni^{2+}-NTA-DOGS = 1057 $\frac{g}{mol}$.

Calculated molar concentration of Vps21 (M):

Ratio of Vps21-His_{10} to outer leaflet Ni^{2+}-NTA-DOGS	mol% of Ni^{2+}-NTA-DOGS: 2	4	4.5	5	6
0.2	6.53E-06	1.30E-05	1.45E-05	1.61E-05	1.93E-05
0.1	3.26E-06	6.48E-06	7.27E-06	8.07E-06	9.64E-06
0.0667	2.18E-06	4.32E-06	4.85E-06	5.38E-06	6.43E-06
0.05	1.63E-06	3.24E-06	3.64E-06	4.03E-06	4.82E-06
0.0167	5.44E-07	1.08E-06	1.21E-06	1.34E-06	1.61E-06
0.0083	2.72E-07	5.40E-07	6.06E-07	6.72E-07	8.04E-07

Rab-His_{10}(M) = outer leaflet Ni^{2+}-NTA-DOGS (M) × Ratio of Vps21-His_{10} to outer leaflet Ni^{2+}-NTA-DOGS.

Calculated molar concentration of liposome (M):

2	4	4.5	5	6
4.16E-08	4.12E-08	4.12E-08	4.11E-08	4.09E-08

$$\text{liposome (M)} = \frac{\text{2.5 g/L lipid}}{760 \times \text{mol\% EggPC} + 1057 \times \text{mol\% } Ni^{2+}\text{-NTA-DOGS}} \times \frac{1}{\text{\# lipid in 100 nm liposome}}$$

$$\text{\# lipid in 100 nm liposome} = \frac{4\pi(50\text{ nm})^2}{0.8\text{ nm}^2} \times 2$$

where 0.8 nm^2 is the estimated surface area of a lipid

Supplementary Table 4 cont'd on next page.

Supplementary Table 4 (cont'd from prev. page)

Upper-bound estimates of Vps21 per μm^2 on liposomes for Fig. 2 and Fig. S1.

mol% Ni^{2+}-NTA-DOGS / Rab-His_{10} : Ni^{2+}-NTA-DOGS	2	4	4.5	5	6
0.2	5,000	10,000	11,250	12,500	15,000
0.1	2,500	5,000	5,625	6,250	7,500
0.0667	1,667	3,333	3,750	4,167	5,000
0.05	1,250	2,500	2,813	3,125	3,750
0.0333	833	1,667	1,875	2,083	2,500
0.0167	417	833	938	1,042	1,250
0.0083	208	417	469	521	625

Vps21· μm^{-2} ≤ mol% Ni^{2+}-NTA-DOGS × number of outer leaflet lipids in liposome × molar ratio of Vps21 to Ni^{2+}-NTA-DOGS / surface area of liposome

- The surface area of a 100 nm diameter liposome is 0.03 μm^2.
- A 100 nm liposome contains 3.9×10^4 lipids in the outer leaflet, assuming 0.8 nm^2 for the surface area of a lipid.
- Since Vps21-His_{10} are anchored onto liposomes through polyhistidine tag interaction with nickel-chelating lipids, the number of membrane-bound Vps21 on a liposome is dependent on the number of Ni^{2+}-NTA-DOGS in the outer leaflet and the molar ratio of Rab-His_{10} to Ni^{2+}-NTA-DOGS.

Supplementary Methods

Reagents

All biochemical reagents were purchased from Sigma-Aldrich or Invitrogen, except as indicated, and were of enzyme grade or better.

Protein expression constructs

Untagged *GYP1*$_{TBC}$ (encoding residues 249-637) was amplified using PCR primers containing engineered BamHI and NcoI restriction sites and cloned into pRSF-1b (Novagen). The *GYP1*$_{TBC\,R343K}$ mutant[7,8] was made by site-directed mutagenesis. *His*$_7$*-MBP-TEV-VPS9* was expressed from a new vector, pAMB585. The multiple cloning site and *MBP* gene from pMBP-Parallel[9] was first cloned into the NcoI and AvrII sites of pRSF-1b (Novagen) using primers containing BsaI sites and the *His*$_7$ 5' sequence, which results in destruction of the original enzyme recognition sites within pRSF-1b. The *VPS9* open reading frame was cloned into pAMB585 using primers containing NcoI and BamHI restriction sites. Rab-His$_{10}$ constructs were amplified using primers containing NcoI and BamH1 restriction sites and encoding the His$_{10}$ sequence, and cloned into pET-19b (Novagen). Since in our experiments recombinant Rabs are anchored to liposomes through the C-terminal His$_{10}$ sequence, the two C-terminal prenyl-acceptor cysteines of Vps21 (C208S C210G) and Ypt7 (C206S C208G) were mutated to preclude the possibility of protein interactions through disulfide bond formation. For preparation of untagged Vps21, an N-terminal chitin binding domain (CBD)-intein cassette was amplified from pTYB11 (NEB) using primers containing a BsmBI restriction site and overlapping *VPS21* sequence. *VPS21* was amplified from *S. cerevisiae* genomic DNA using primers containing a NotI restriction site and overlapping intein-chitin binding domain sequence. Both overlapping PCR products were fused by subsequent PCR amplification using primers containing BsmBI and NotI restriction sites and cloned into NcoI and NotI sites of pRSF-1b (Novagen). The two C-terminal prenyl-acceptor cysteines of Vps21 were mutated (C208G C210G).

Rab-His_{10} expression and purification

Rab-His_{10} was expressed in *E. coli* BL21 (DE3) and grown in TB medium containing ampicillin to OD_{600} = 1.5-2.5. Protein expression was induced with 0.1 mM IPTG at 16° C overnight. Cells were lysed by sonication on ice in 50 mM sodium phosphate, pH 7.4, 20 mM imidazole, pH 7.4, and 500 mM NaCl supplemented with protease inhibitors (PMSF, leupeptin, and pepstatin), lysozyme, and DNaseI. Protein was affinity purified on HisTrap FF column (GE Healthcare) according to the manufacturer's recommendations, and eluted with 250-500 mM imidazole from a linear imidazole gradient. Fractions containing Rab-His_{10} fusion proteins were pooled and further purified by size exclusion chromatography on Superdex 75 (GE Healthcare) pre-equilibrated with 20 mM HEPES · NaOH, pH 7.5, 150 mM NaCl, and 2 mM 2-mercaptoethanol. GDP, $MgCl_2$, and glycerol were then added to final concentrations of 1 mM, 3 mM and 5% (v/v). Fractions collected from the major peak were concentrated using an Amicon Ultra-15 concentrator 10,000 MWCO (Millipore). Protein aliquots were flash-frozen in liquid N_2 and stored at −80°C. The resulting Vps21 preparations were monodisperse (Supplementary Fig. 1) and exhibited robust activity when tested for GAP-stimulated single-round GTP hydrolysis (Supplementary Fig. 4).

Untagged Vps21 expression and purification

CBD-intein-Vps21 was expressed in *E. coli* BL21 (DE3) and grown in TB containing ampicillin to OD_{600} = 1.5-2.5. Protein expression was induced with 0.1 mM IPTG at 16°C overnight. Cells were harvested and then lysed by sonication on ice in 20 mM HEPES · NaOH, pH 7.4, and 500 mM NaCl, supplemented with protease inhibitors, lysozyme, and DNase I. Vps21 was affinity purified using chitin resin (NEB) according to the manufacturer's recommendations. After incubating clarified cell lysate with chitin resins for 4 hours, the resins were washed extensively with 20 mM HEPES · NaOH, pH 7.4, and 500 mM NaCl. On-column cleavage was performed in 20 mM HEPES · NaOH, pH 7.4, 500 mM NaCl, and 50 mM dithiothreitol overnight at room temperature. $MgCl_2$ was added to the eluted sample to a final concentration of 1 mM and incubated for 30 minutes before further purification by size exclusion chromatography on Superdex 75 (GE Healthcare) pre-equilibrated with 20 mM HEPES · NaOH, pH 7.5, 150 mM NaCl, and 1mM $MgCl_2$. Fractions collected from the major peak were concentrated using an Amicon Ultra-15 concentrator 10,000 MWCO (Millipore).

GDP, $MgCl_2$, and glycerol were added to the final concentrations of 1 mM, 3 mM and 5% (v/v). Protein aliquots were flash-frozen in liquid N_2 and stored at –80°C.

$Gyp1_{TBC}$ expression and purification

$Gyp1_{TBC}$ was expressed in *E. coli* BL21 (DE3) pRIL and grown in TB medium containing kanamycin and chloramphenicol to OD_{600} = 1.5-2.5. Protein expression was induced with 0.1 mM IPTG at 25°C overnight. Cells were lysed by sonication on ice in 50 mM sodium phosphate, pH 7.4, 150 mM NaCl, and 2 mM 2-mercaptoethanol supplemented with protease inhibitors, lysozyme, and DNaseI. Ice-cold saturated ammonium sulfate (SAS) was added to the clarified lysate to a final concentration of 25% (v/v), and rocked at 4°C for 1 hour. Precipitated material was removed by sedimentation and discarded, and additional SAS was added to a final concentration of 35% (v/v) and rocked at 4°C for 1 hour. The precipitate from the 25-35% (v/v) SAS cut was sedimented, then the pellet was washed gently with cold water and resuspended into 20 mM phosphate buffer, pH 7.4. The resulting material was separated by ion exchange chromatography on Source Q column (GE Healthcare). $Gyp1_{TBC}$ was eluted using a linear NaCl gradient in a 20 mM Tris · HCl, pH 7.5, base buffer, with peak fractions eluting at 170-240 mM NaCl pooled and further purified by size exclusion on Superdex 75 pre-equilibrated with 20 mM HEPES · NaOH, pH 7.5, 150 mM NaCl, and 2 mM 2-mercaptoethanol. Fractions collected from the major peak were concentrated using an Amicon Ultra-15 concentrator 10,000 MWCO (Millipore). Protein aliquots were flash-frozen in liquid N_2 and stored at –80°C. The same procedure was used to prepare $Gyp1_{TBC\text{-}R343K}$. GAP activity in solution of these Gyp1 preparations is shown in Supplementary Fig. 4.

Vps9 expression and purification

Vps9 expression and purification was modified from a published procedure[10]. His_7-MBP-TEV-Vps9 was expressed in *E. coli* BL21 (DE3) pRIL and grown in TB medium with kanamycin and chloramphenicol to OD_{600} = 1.5-2.5. Protein expression was induced with 0.1 mM IPTG at 25°C overnight. Cells were lysed by sonication on ice in 50 mM sodium phosphate, pH 7.4, 150 mM NaCl, 2 mM 2-mercaptoethanol supplemented with protease inhibitors, lysozyme, and DNaseI. His_7-MBP-TEV-Vps9 was first affinity purified by amylose affinity chromatography. Vps9 bound to the amylose resin was washed extensively with 50 mM sodium phosphate, pH

7.4, 150 mM NaCl and 2 mM 2-mercaptoethanol before elution with 50 mM sodium phosphate buffer, pH 7.4, 150 mM NaCl, and 10 mM maltose. EDTA and dithiothreitol were added to 0.5 mM and 1 mM, respectively, to His_7-MBP-TEV-Vps9 before overnight incubation with 0.2 molar excess His_6-TEV protease at 16° C. Overnight TEV-cleaved products were diluted with 50mM phosphate buffer, pH 7.4, until NaCl concentration was less than 100 mM, and loaded onto a Source Q ion exchange column (GE Healthcare). Vps9 eluted from column at 20 mM Tris · HCl, pH 7.5, and 180-280 mM NaCl, using a linear NaCl gradient. Residual uncleaved His_7-MBP-TEV-Vps9 and His_6-TEV protease were removed with a HisTrap Ni FF column pre-equilibrated with 25 mM Tris · HCl, pH7.5, 20 mM imidazole, pH 7.5, and 150 mM NaCl. Vps9 was buffer exchanged by ultrafiltration into 20 mM HEPES · NaOH, pH 7.5, 150 mM NaCl, and 2 mM 2-mercaptoethanol using an Amicon Ultra-15 concentrator (Millipore). Protein aliquots were flash-frozen in liquid N_2 and stored at –80°C. GEF activity in solution of the purified Vps9 is shown in Supplementary Fig. 4.

Quasielastic light scattering (QLS)

Measurements were performed using a Brookhaven 90 Plus Particle Size Analyzer (Brookhaven Instruments Cooperation; BIC) at a fixed angle of 90° for 1 minute at 25°C. The autocorrelation functions derived from scattering intensity data were analyzed using the cumulant method[11] to yield a polynomial description of the distribution. The first two moments of this polynomial provide the effective hydrodynamic diameter (the main parameter reported in our study) and a distribution width (polydispersity) of the liposomes in solution. For all the QLS experiments, polydispersity values were not reported since the majority of samples in which substantial tethering was occurring displayed a polydispersity value >0.8, indicating a broad size distribution. The liposome size distributions (Fig. 8) were represented by the relative scattering intensity as a function of particle size, obtained by fitting a non-negative least squares algorithm to the autocorrelation function followed by regularization to relate the intensity peaks to inferred diffusion coefficients of the particles in the suspension, as descibed[12]. These analyses were performed using the BIC particle sizing software.

The intensity of scattering is roughly proportional to the square of particle diameter. To evaluate the sensitivity of the effective diameter parameter to different mixtures of particle

size, we performed calibration experiments. Bare liposomes were extruded through filters having nominal pore diameters of 50, 100, and 800 nm. Each population, and defined binary mixtures of pairs of populations were prepared (e.g., 40% ~50 nm liposomes plus 60% ~100 nm liposomes by mass), and measured by QLS. These experiments demonstrated that the assay is robust and, at lower levels of tethering, relatively linear. First, the assay is sensitive to small changes in particle size: for particles with diameters of <200nm, a two-fold increase in the effective diameter of 20% (by mass) of the population is readily detectible. Second, in the small 50-200 nm size range, the relationship between the mass fraction of larger and smaller particles and the measured effective diameter is linear ($r^2 = 0.995$). Third, when ~100 nm liposomes are mixed with larger ~1000 nm liposomes, the relationship between mass fraction and effective diameter remains almost linear at ~1000 nm liposome mass fractions up to 60%. These experiments, and classical experiments using highly uniform polystyrene beads, show that effective diameter provides a useful measure of tethering activity in a vesicle or liposome population[11,12].

Tethering cooperativity analysis

For the analysis of Vps21 cooperativity in tethering, sets of liposomes containing different amounts of Ni^{2+}-NTA-DOGS were prepared and each population was decorated with various amounts of Vps21. The effective diameter for each population was measured by QLS after a 60 min incubation, and the effective diameter data were plotted vs. upper-bound estimates of Vps21 surface density (Supplementary Fig. 2 and Table 4). Nonlinear least-squares fitting of the Hill equation to the resulting family of curves was then performed in GraphPad Prism. Individual fits yielded cooperativity coefficients similar to the global fit, which is the value reported in the text. The value reported in the text is the lower boundary of a one-tailed 95% confidence limit. An important caveat in this experiment is that most of the tethering reactions (particularly at higher Vps21 surface densities) had not reached equilibrium. Effective particle diameters continued to increase at these higher Rab densities for several hours. Thus, even the reported cooperativity coefficient is likely an underestimate.

Size-exclusion chromatography and multi-angle light scattering (SEC-MALS)

Vps21 or Vps21-His_{10} was preloaded with GTP or GDP as described in the liposome tethering assay procedure and buffer exchanged into MALS buffer (20 mM HEPES · NaOH, pH 7.5, 150 mM NaCl, and 1 mM $MgCl_2$). 100 µl of nucleotide-loaded Rab at 5 $mgml^{-1}$ (~200 µM) was injected into a Superdex 75 10/300 GL column (~24 ml total volume, GE Healthcare) equilibrated with MALS buffer at a flow rate of 0.5 ml per min. The SEC column was connected in line with a miniDAWN TREOS light scattering detector (658 nm, Wyatt Technologies). Data were collected and evaluated using ASTRA software (version 5.3.4; Wyatt Technologies) using a dn dc^{-1} value of 0.185 ml g^{-1} and a protein extinction coefficient calculated based on amino acid sequence and the GTP or GDP extinction coefficient.

GAP and GEF activity assays

The GTP hydrolysis assay was modified from a published procedure [8]. GAP and GEF proteins were buffer exchanged into 20 mM HEPES · NaOH, pH 7.5, and 150 mM NaCl. GTP-loaded Rab-His_{10} was prepared as described in the liposome tethering assay except that 1 mM $MgCl_2$ and 2 mM 2-mercaptoethanol were eliminated from the reaction buffer. Inorganic phosphate released by single- or multiple-turnover GTP hydrolysis was continuously monitored using EnzChek Phosphate Assay Kit (Invitrogen) adapted to a 100 µl reaction volume in 96-well half-area plates (Corning). 25 µl of GTP-loaded Rab-His_{10} was added to 75 µl assay buffer, with or without GAP and GEF proteins added as indicated to initiate the assay. Each reaction contained a final concentration of 20 mM HEPES · NaOH, pH 7.5, 150 mM NaCl, 10 mM $MgCl_2$, 0.2 mM GTP, 0.15 mM 2-amino-6-mercapto-7-methylpurine ribonucleoside, 0.75 U ml^{-1} purine nucleoside phosphorylase, 20 µM GTP-loaded Rab-His_{10}, and GAP and GEF proteins at the indicated concentrations. Absorbance at 360 nm measured using a Perkin Elmer Victor 3 plate reader.

Estimation of *in vivo* Rab surface densities

Our estimate of the density of Rab3a on synaptic vesicles is derived from work on the protein composition of purified synaptic vesicles by Takimori and colleagues[14]. In these preparations, each purified synaptic vesicle bore an average of 10.3 molecules of Rab3a, and the vesicles had a measured mean outer diameter of 41.6 nm, giving a surface area of 0.0054 μm^2 and therefore

~1,950 Rab3a μm^{-2} of membrane. By comparison, the Ca^{2+} sensor protein synaptotagmin was present at ~2,800 μm^{-2}.

Our estimate of the density of Ypt7 on the yeast vacuole is based on measurements of the relative abundances of vacuolar fusion proteins[15] and of absolute per-cell protein copy numbers[16]. In previous work, we GFP-tagged many resident vacuolar proteins, expressing the fusions from native chromosomal loci, and demonstrated that the tagged proteins were functional. Using antibodies against the native proteins, we demonstrated that each GFP-tagged fusion was expressed at the same level as the untagged version. Finally, we used quantitative immunoblotting with anti-GFP antibodies to estimate the relative abundances of each tagged vacuolar fusion factor, in whole cells and on preparations of purified yeast vacuoles[15]. In separate work, quantitative immunoblotting was used to estimate absolute per-cell abundances of most yeast proteins. For vacuolar proteins, the relative abundances obtained in both studies agreed closely, generally to within 1.5-fold. Based on these combined data sets, we estimate that an average yeast cell contains ~5,500 molecules of Ypt7. Both subcellular fractionation and fluorescence microscopy demonstrate that ≥90% of Ypt7 is on vacuole membranes, indicating that ~5000 copies of Ypt7 are found on vacuole membranes in each cell. Vacuoles are large (typically >1μm in diameter), and the standard method of vacuole purification begins with a hypotonic wash that causes all vacuoles in each cell to fuse prior to cell lysis[17,18]. Thus, each purified vacuole in the final preparation consists of the fusion product of most or all vacuoles from a single cell. By light microscopy the mean diameter of these spherical vacuoles is 2.0 μm, and by QLS, the effective diameter is 1.8 μm[18]. Estimates of the vacuole area in living cells give comparable results. Based on a spherical diameter of 1.9 μm, an average cell contains ~10 μm^2 of vacuolar membrane bearing ~5000 copies of Ypt7. Hence, the *in vivo* Ypt7 surface density is ~500 μm^{-2}.

Estimation of Rab tether lengths

The C-terminal linkers that tether Rab proteins to membranes are largely unordered, allowing the membrane-anchored Rab's GTP-binding domain to extend some distance from the bilayer surface. Studies using several techniques, including Förster resonance energy transfer, force spectroscopy, and electron microscopy show that unordered polymers including nucleic acids,

denatured proteins, and intrinsically unstructured polypeptides behave as entropic springs[19-23]. The mechanical properties of such polymers are usefully described by the worm-like chain (WLC) model. The contour length L_C of a linker N residues long is:

$$L_C = N \times 0.38 \text{ nm}$$

where 0.38 nm is the residue-to-residue distance in a fully extended polypeptide. For unstructured polypeptides, the characteristic persistence length L_P – the distance over which orientations of segments of the chain are uncorrelated – is typically in the range of 0.4-0.6 nm. Using these values, it is possible to estimate the relationship between tensile force F and chain elongation x:

$$F = kT / L_P \left[{}^1\!/_4 \left(1 - x / L_C\right)^{-2} - {}^1\!/_4 + x / L_C \right]$$

where k is the Boltzmann constant and T is temperature[21].

Our experiments show that the Rab-Rab bonds involved in tethering must be switchable, *i.e.*, they dissociate when GDP rather than GTP is bound. Although the rupture force for Rab-Rab (or Rab-effector) bonds is unknown, similar bond rupture events have been analyzed in detail using force spectroscopy: the unbinding of rigor-bound kinesin and myosin heads from microubules and microfilaments[24-26]. These bonds, like Rab-Rab and Rab-effector bonds, are strictly controlled by bound nucleotides (ATP and ADP), and fail (rupture) under applied forces in the 5-10 pN range. It is therefore unlikely that a GTP-regulated Rab-Rab or Rab-effector complex can remain associated under tensile loads greater than ~10 pN.

For a 35-residue linker with L_P = 0.5 nm, at x = 4 nm the predicted force is ~5 pN, and at x = 6 nm it is ~10 pN. For a Rab-Rab dimer spanning a pair of tethered membranes, then, the intermembrane distance will be 2x: probably not more than 12 nm near the rupture force, and closer to 6-8 nm at lower forces. To this distance we must add any length contributed by the Rab globular heads. Depending on the binding geometry, this could be from zero to 5 nm. Hence, the longest plausible GTP-regulated Rab-Rab tether would rupture at an intermembrane separation of ~17 nm. At lower tether forces the intermembrane distance should be closer to 8-11 nm, as discussed in the main text. We note that in a related application of the WLC model, Tareste and colleagues[27] estimated the number of unstructured residues in a partially-zipped *trans*-SNARE complex at an intermembrane distance of ~8 nm (see Fig. 4D

in the present study). The results of Tareste *et al.* are fully consistent with our group's studies of the assembly of partially-zipped *trans*-SNARE complexes using intact yeast vacuoles[28].

Supplementary References

1. Peterson, M. R., Burd, C. G. & Emr, S. D. Vac1p coordinates Rab and phosphatidylinositol 3-kinase signaling in Vps45p-dependent vesicle docking/fusion at the endosome. *Curr. Biol.* **9**, 159-162 (1999).
2. Tall, G. G., Hama, H., DeWald, D. B. & Horazdovsky, B. F. The phosphatidylinositol 3-phosphate binding protein Vac1p interacts with a Rab GTPase and a Sec1p homologue to facilitate vesicle-mediated vacuolar protein sorting. *Mol. Biol. Cell* **10**, 1873-1889 (1999).
3. Peplowska, K., Markgraf, D. F., Ostrowicz, C. W., Bange, G. & Ungermann, C. The CORVET tethering complex interacts with the yeast Rab5 homolog Vps21 and is involved in endo-lysosomal biogenesis. *Dev. Cell* **12**, 739-750 (2007).
4. Hama, H., Tall, G. G. & Horazdovsky, B. F. Vps9p is a guanine nucleotide exchange factor involved in vesicle-mediated vacuolar protein transport. *J. Biol. Chem.* **274**, 15284-15291 (1999).
5. Horazdovsky, B. F., Busch, G. R. & Emr, S. D. VPS21 encodes a rab5-like GTP binding protein that is required for the sorting of yeast vacuolar proteins. *EMBO J.* **13**, 1297-1309 (1994).
6. Calero, M. et al. Dual prenylation is required for Rab protein localization and function. *Mol. Biol. Cell* **14**, 1852-1867 (2003).
7. Albert, S., Will, E. & Gallwitz, D. Identification of the catalytic domains and their functionally critical arginine residues of two yeast GTPase-activating proteins specific for Ypt/Rab transport GTPases. *EMBO J.* **18**, 5216-5225 (1999).
8. Pan, X., Eathiraj, S., Munson, M. & Lambright, D. G. TBC-domain GAPs for Rab GTPases accelerate GTP hydrolysis by a dual-finger mechanism. *Nature* **442**, 303-306 (2006).
9. Sheffield, P., Garrard, S. & Derewenda, Z. Overcoming expression and purification problems of RhoGDI using a family of "parallel" expression vectors. *Protein Expr Purif* **15**, 34-39 (1999).
10. Davies, B. A., Carney, D. S. & Horazdovsky, B. F. Ubiquitin regulation of the Rab5 family GEF Vps9p. *Methods Enzymol.* **403**, 561-583 (2005).
11. Brown, J. C., Pusey, P. N. & Dietz, R. Photon correlation study of polydisperse samples of polystyrene in cyclohexane. *The Journal of Chemical Physics* **62**, 1136 (1975).
12. Lomakin, A., Teplow, D. B. & Benedek, G. B. Quasielastic light scattering for protein assembly studies. *Methods Mol. Biol.* **299**, 153-174 (2005).
13. Brett, C. L. et al. Efficient termination of vacuolar Rab GTPase signaling requires coordinated action by a GAP and a protein kinase. *J. Cell Biol.* **182**, 1141-1151 (2008).
14. Takamori, S. et al. Molecular anatomy of a trafficking organelle. *Cell* **127**, 831-846 (2006).
15. Wang, L., Seeley, E. S., Wickner, W. & Merz, A. J. Vacuole fusion at a ring of vertex docking sites leaves membrane fragments within the organelle. *Cell* **108**, 357-369 (2002).
16. Ghaemmaghami, S. et al. Global analysis of protein expression in yeast. *Nature* **425**, 737-741 (2003).
17. LaGrassa, T. J. & Ungermann, C. The vacuolar kinase Yck3 maintains organelle fragmentation by regulating the HOPS tethering complex. *J. Cell Biol.* **168**, 401-414 (2005).

18. Brett, C. L. & Merz, A. J. Osmotic regulation of Rab-mediated organelle docking. *Curr. Biol.* **18**, 1072-1077 (2008).
19. Zhou, H. X. Polymer models of protein stability, folding, and interactions. *Biochemistry* **43**, 2141-2154 (2004).
20. Linke, W. A. et al. PEVK domain of titin: an entropic spring with actin-binding properties. *J. Struct. Biol.* **137**, 194-205 (2002).
21. Bustamante, C., Marko, J. F., Siggia, E. D. & Smith, S. Entropic elasticity of lambda-phage DNA. *Science* **265(5178)**, 1599-1600 (1994).
22. Ohashi, T., Galiacy, S. D., Briscoe, G. & Erickson, H. P. An experimental study of GFP-based FRET, with application to intrinsically unstructured proteins. *Protein Sci* **16**, 1429-1438 (2007).
23. Evers, T. H., van Dongen, E. M., Faesen, A. C., Meijer, E. W. & Merkx, M. Quantitative understanding of the energy transfer between fluorescent proteins connected via flexible peptide linkers. *Biochemistry* **45**, 13183-13192 (2006).
24. Oguchi, Y. et al. Load-dependent ADP binding to myosins V and VI: implications for subunit coordination and function. *Proc. Natl. Acad. Sci. U S A* **105**, 7714-7719 (2008).
25. Uemura, S. et al. Kinesin-microtubule binding depends on both nucleotide state and loading direction. *Proc. Natl. Acad. Sci. U S A* **99**, 5977-5981 (2002).
26. Kawaguchi, K. & Ishiwata, S. Nucleotide-dependent single- to double-headed binding of kinesin. *Science* **291**, 667-669 (2001).
27. Li, F. et al. Energetics and dynamics of SNAREpin folding across lipid bilayers. *Nat Struct Mol Biol* **14**, 890-896 (2007).
28. Schwartz, M. L. & Merz, A. J. Capture and release of partially zipped trans-SNARE complexes on intact organelles. *J. Cell Biol.* **185**, 535-549 (2009).